A Generic, Geometric Approach to Accurate Machining-Error Predictions for 3-Axis CNC Milling of Sculptured Surface Parts

Wei Cai

M.A.Sc. Thesis

in

The Department

of

Mechanical and Industrial Engineering

Presented in Partial Fulfillment of the Requirements

for the Degree of Master of Applied Science (Mechanical Engineering) at

Concordia University

Montreal, Quebec, Canada

October 2005

Your file Votre référence
ISBN: 0-494-14300-2
Our file Notre référence
ISBN: 0-494-14300-2

Supervisor: Dr. Zezhong Chevy Chen

Abstract

A Generic, Geometric Approach to Accurate Machining-Error Predictions
for 3-Axis CNC Milling of Sculptured Surface Parts

The goal of computer numerical control (CNC) machining for sculptured part finishing is to ensure the required-surface quality while maintaining maximum machining efficiency. This work addresses these challenging and conflicting tasks that demand more research.

In CNC machining, machining errors are usually caused by some of the sources such as cutting tool deflection, cutting tool wear, machine tool vibration, improper coolant, improper lubrication, and negative thermal effect. To increase product accuracy, much research has been carried out on the prediction of machining errors by the above sources. However, in milling of sculptured surface parts, due to their curved shapes, the geometries of cutting tools do not match the parts' surfaces well if the tools cut along the tool paths on the surfaces in a point-to-point way. As a consequence, machining error is inevitable, even if there is no other source of error in ideal machining conditions. To predict machining errors caused by this tool-surface mismatch, several methods have been proposed. Some of them are simple, and some represent the geometry of machined surfaces using cutter-swept surfaces. But none of these methods is accurate and practical.

In this thesis research work, a generic, geometric approach to predicting accurate machining errors caused by the tool-surface mismatch is proposed for 3-axis sculptured

surface milling. To implement this new approach, a cutter contact (CC) point optimization system is also proposed for optimizing CC points along tool paths to ensure adequate surface quality without surface gouging. A semi-cylindrical part and a Non-Uniform Rational B-Spline (NURBS) surface part are used to illustrate this approach and to demonstrate its superiority.

This thesis research work provides a profound understanding of the machining errors caused by the tool-surface mismatch. It not only contributes to tool path planning for 3-axis CNC milling of sculptured surface parts, but also has potential to benefit the aeronautic, automotive and die/mold manufacturing industries.

Table of Contents

Abstract iii
Table of Contents v
List of Tables vii
List of Figures viii
Acknowledgements xi

Chapter 1 Introduction 1

1.1 Sculptured surface parts 1
1.2 CAD/CAE/CAM of sculptured parts 6
1.3 Three-axis CNC machining of sculptured parts 9
1.4 Machining-error predictions for three-axis CNC milling of sculptured parts 12
1.5 Cutter contact point determination in three-axis CNC milling of sculptured parts 14
1.6 Objectives of this thesis 16
1.7 Outline of this thesis 17

Chapter 2 Cutter-Swept Surface Modeling and Formulation 18

2.1 Geometric model of furrow patches of machined surfaces 18
2.1.1 Geometric model of furrow patches machined using flat end-mills 19
2.1.2 Geometric model of furrow patches machined using APT tools 23
2.2 Envelope of cutting circles 26
2.3 Machining-error predictions 32
2.4 Examples 35

Chapter 3 Application: CC Point Optimization System 42

3.1 Introduction to two established CC point generation methods 42
3.1.1 The chordal deviation method and circular arc approximation method 43

3.1.2 Limitations of the established CC point generation methods.....45
3.2 Sensitivity study of machining error with respect to tools.....47
3.2.1 Relationship between machining error and tool type.....47
3.2.2 Relationship between machining error and tool size.....51
3.3 CC point optimization system.....54
3.3.1 Optimization procedure.....54
3.3.2 Case study and analysis.....55
Chapter 4 Summary and Contributions 68
Bibliography 70
Publications 74

List of Tables

Table 2.1 Predicted maximum machining errors in the selected tool steps by the three methods....38

Table 2.2 Predicted maximum machining errors of the local surface areas using different methods....40

Table 3.1 Maximum machining errors using the three tools in the selected tool steps for the semi-cylindrical surface machining....49

Table 3.2 Maximum machining errors using the three tools in the selected tool steps for the sculptured surface machining....50

Table 3.3 Maximum machining errors using ball end-mills of different sizes in the selected steps....52

Table 3.4 Maximum machining errors using flat end-mills of different sizes in the selected steps....53

List of Figures

Figure 1.1 A NURBS surface patch.....4

Figure 1.2 Sculptured surface of a mouse.....5

Figure 1.3 (a) Ferrari formula one racing car; (b) turbines of airplane engines. 6

Figure 1.4 (a) 3D solid model of a race car; (b) stress distribution of a pair of gears; (c) machining simulation of a handset die. 9

Figure 1.5 Three types of common milling cutters. (a) Ball end-mill; (b) torus end-mill; (c) flat end-mill.....11

Figure 1.6 Diagram of a 3-axis CNC vertical milling machine.....11

Figure 2.1 (a) APT tool; (b) torus end-mill ($\alpha = 0$ and $\beta = 0$); (c) ball end-mill ($\alpha = 0$, $\beta = 0$, and $R_1 = 0$); (d) flat end-mill ($\alpha = 0$, $\beta = 0$, and $R_2 = 0$).....20

Figure 2.2 Geometric model of furrow patches. (a) A flat end-mill step in surface milling; (b) the envelope of the cutting circles on layer (z). 22

Figure 2.3 Geometric model of furrow patches. (a) An APT tool step; (b) the envelope of cutting circles on layer Ω; (c) the envelope of cutting circles on layer Π. 25

Figure 2.4 APT tool in the part and cutter coordinate systems.....27

Figure 2.5 Cutting circles in different cutting surfaces in the cutter coordinate system. .29

Figure 2.6 Illustration of machining-error predictions. (a) Cutter-swept surface between two CC points; (b) surface contour and an envelope of cutting circles on a layer; (c) projection of the envelope and the surface contour. 34

Figure 2.7 Six tool paths on a regular semi-cylindrical surface part. 36

Figure 2.8 Furrow patch between two CC points on the semi-cylindrical surface part....36

Figure 2.9 Selected CC points of five tool steps on the NURBS surface. 39

Figure 3.1 Illustration of the chordal deviation method. 43

Figure 3.2 Model of machining errors in the circular arc approximation method....44

Figure 3.3 Geometric characteristics of sculptured surface milling. 46

Figure 3.4 Six pairs of sample CC points on the semi-cylindrical surface in the sensitivity study. 48

Figure 3.5 Five pairs of sample CC points on the sculptured surface in the sensitivity study. 50

Figure 3.6 Semi-cylindrical surface part with iso-parametric tool paths. 56

Figure 3.7 CC points on a tool path determined by (a) the circular arc approximation method or the optimization system; (b) the chordal deviation method. 57

Figure 3.8 Machined surface of the semi-cylinder in simulation. 58

Figure 3.9 Predicted machining errors at the sample points along one tool path from the two regions. 58

Figure 3.10 (a) Machined semi-cylindrical surface part; (b) the semi-cylindrical surface part measured on a CMM. 59

Figure 3.11 Measured machining errors of the left-hand region 61

Figure 3.12 Measured machining errors of the right-hand region. 61

Figure 3.13 CC points on iso-parametric tool paths of the sculptured surface determined by (a) the circular arc approximation method; (b) the CC point optimization system. 62

Figure 3.14 Sculptured surface machined with the CC points determined with the chordal deviation method. 64

Figure 3.15 Sculptured surface machined with the CC points determined with the circular arc approximation method.....64

Figure 3.16 Sculptured surface machined with the CC points optimized with the CC point optimization system.....65

Figure 3.17 Predicted machining errors along the middle tool path using the three methods.....65

Figure 3.18 Predicted machining errors along the outmost tool path using the three methods.....66

Figure 3.19 Machined part.....67

Acknowledgements

First and foremost, I would particularly like to express my sincere gratitude to my supervisor, Dr. Zezhong Chevy Chen, for his guidance, academic suggestions, financial support as well as encouragement throughout all my study. Without his in-depth and extensive understanding in this professional field, the fulfillment of my thesis would not have been achieved.

Also I owe special thanks to Prof. Xujing Yang from Hunan University in China for his help. Besides those who have directly assisted me with this work, I would like to acknowledge the technical support staff in the department machine shop, especially to the machine shop supervisor, Mr. Brian Cooper, and the machinist, Mr. Alex Macpherson, for their kindness when I was doing experiments.

Last but not least, I would like to thank my wonderful parents for their insight and inspiration.

Chapter 1 Introduction

1.1 Sculptured surface parts

Mechanical parts with sculptured or freeform surfaces called sculptured parts have been broadly used in today's industries, such as automobile, aircraft, and die/mold manufacturing. A free-form surface is a family of untrimmed surface patches that interconnect while maintaining tangency (G^1) or curvature (G^2) continuity on their conjunction boundaries. Each surface patch can be mathematically approximated via various parametric surface patches which are classified into Bilinear surface, Coon's patch, Bi-cubic surface, Bezier surface, B-spline, and Non-Uniform Rational B-Spline (NURBS) surface. Among these patches, the NURBS surface equation is a general form that includes B-spline surface equation and is able to exactly represent the quadratic cylindrical, conical, spherical, paraboloidal, and hyperboloidal surfaces. Therefore, the NURBS surface equation often serves as a unified internal representation for all these surfaces [1]. A NURBS surface of degree (k,l) is defined by

$$\mathbf{P}(u,v)=\frac{\sum_{i=0}^{n}\sum_{j=0}^{m} w_{i,j}\cdot\mathbf{P}_{i,j}\cdot N_{i,k}(u)\cdot N_{j,l}(v)}{\sum_{i=0}^{n}\sum_{j=0}^{m} w_{i,j}\cdot N_{i,k}(u)\cdot N_{j,l}(v)} \qquad (s_{k-1}\le u\le s_{n+1},\ t_{l-1}\le v\le t_{m+1}) \quad (1.1)$$

where u and v are two parameters (see Fig. 1.1). $\mathbf{P}_{i,j}$ are the control points located at the vertices of the control polyhedron. $w_{i,j}$ are the homogeneous coordinates of the control points. $N_{i,k}(u)$ and $N_{j,l}(v)$ are the nonrational B-spline blending functions which are defined by the following recursive formulas

$$N_{i,k}(u) = \frac{(u - s_i) \cdot N_{i,k-1}(u)}{s_{i+k-1} - s_i} + \frac{(s_{i+k} - u) \cdot N_{i+1,k-1}(u)}{s_{i+k} - s_{i+1}} \tag{1.2}$$

$$N_{i,1}(u) = \begin{cases} 1 & s_i \le u \le s_{i+1} \\ 0 & otherwise \end{cases} \tag{1.3}$$

$$N_{j,l}(v) = \frac{(v - t_j) \cdot N_{j,l-1}(v)}{t_{j+l-1} - t_j} + \frac{(t_{j+l} - v) \cdot N_{j+1,l-1}(v)}{t_{j+l} - t_{j+1}} \tag{1.4}$$

$$N_{j,1}(v) = \begin{cases} 1 & t_j \le v \le t_{j+1} \\ 0 & otherwise \end{cases} \tag{1.5}$$

where s_i and t_j usually refer to the nonperiodic knot values which range from s_0 to s_{n+k} and from t_0 to t_{m+l}, respectively. They are determined from

$$s_i = \begin{cases} 0 & 0 \le i \le k \\ i - k + 1 & k \le i \le n \\ n - k + 2 & n \le i \le n + k \end{cases} \tag{1.6}$$

$$t_j = \begin{cases} 0 & 0 \le j \le l \\ j - l + 1 & l \le j \le m \\ m - l + 2 & m \le j \le m + l \end{cases} \tag{1.7}$$

A NURBS surface patch is shown in Fig. 1.1.

NURBS (Non-Uniform Rational B-Spline) are industry standard tools for the representation and design of geometry. Some reasons for the use of the NURBS surfaces are that they [2]:

- provide a unified mathematical basis for representing both standard analytical shapes (e.g. conics) and freeform surfaces,
- provide the flexibility to design a large variety of shapes,
- can be evaluated reasonably fast by numerically stable and accurate algorithms,
- are invariant under common geometric transformations, and
- are generalizations of rational Bezier and B-spline surfaces.

Due to these advantages, in our research work NURBS surface is employed to implement applications and simulations.

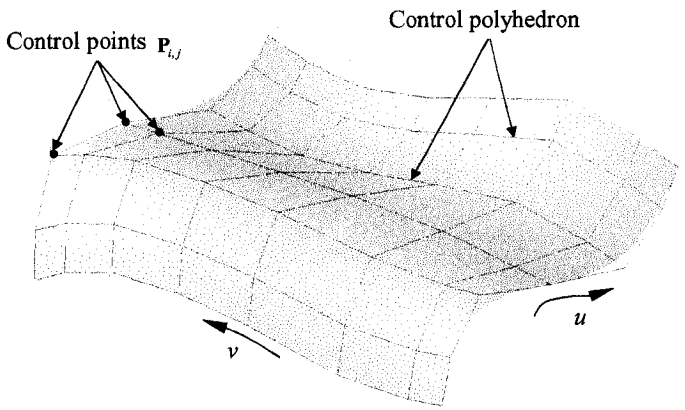

Figure 1.1 A NURBS surface patch.

Unlike planar and natural quadric surfaces such as cylindrical, spherical, and conical surfaces, the main feature of a surface patch is that the surface normals at points on the patch vary from point to point. Because the patches are in curved form, the sculptured surfaces can represent very complex shapes in design. The computer mouse (see Fig. 1.2) is a simple example of a sculptured surface. Compared to the prismatic parts, sculptured parts can provide ergonomic, aerodynamic, or hydrodynamic functionality.

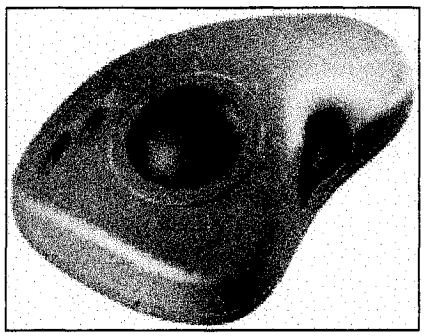

Figure 1.2 Sculptured surface of a mouse.

Sculptured parts have been frequently used everywhere in our daily lives. Electronics (e.g., MP3 players, television sets, razors, and speakers, etc.,) employ many plastic sculptured parts for popular aesthetic appearances. To make these parts, the injection molds should be sculptured as well. The body of the Ferrari-Formula-One racing car in Fig. 1.3(a) is also a typical metal sculptured part which is designed with taking into account product aesthetics, fluid dynamics, and robustness. The die to manufacture this metal body is sculptured which requires high precision. Moreover, the sculptured parts play a more important role in the aeronautics industry. For example, the turbine blades (see Fig. 1.3(b)) in airplane engines utilize aerodynamic shapes to increase the efficiency of the engine. Because of the popularity and importance of sculptured parts in today's industries, designing and manufacturing them efficiently is in high demand and benefits our lives.

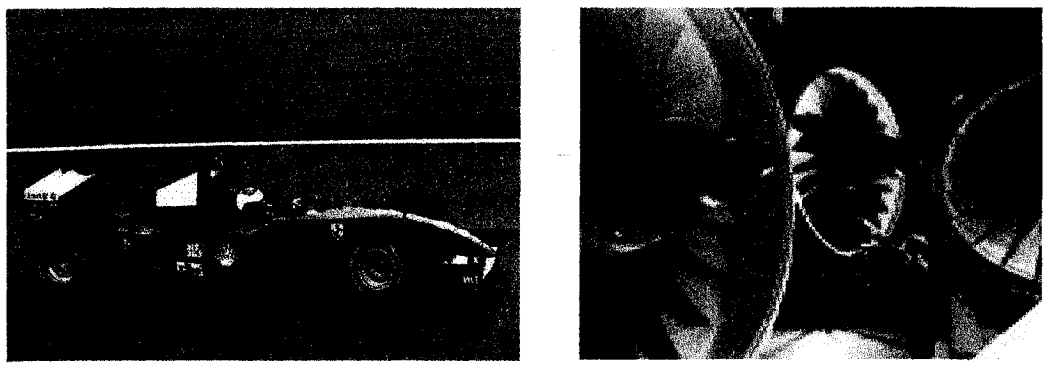

(a) (b)

Figure 1.3 (a) Ferrari formula one racing car; (b) turbines of airplane engines.

1.2 CAD/CAE/CAM of sculptured parts

Before the advent of high-speed computation and the progress of numerically controlled (NC) machines, the sculptured surfaces were produced by artisans who made a master model of clay or wood by hand according to the product aesthetics. The master models were regarded as the "databases" for different types of sculptured surfaces and stored in a dry and climate-controlled warehouse. For the purpose of mass production of sculptured parts, dies and molds were used for producing metal and polymer parts, respectively. At that time, the dies and molds were milled by a tool cutter moving along the duplicated paths as a stylus traced on the surfaces of the master model. This traditional method caused three major disadvantages: (1) the storage of the clay or wood models demanded a huge space; (2) the design and local modification of sculptured surfaces were inconvenient; (3) the machining procedure of the surfaces decreased the finished surface accuracy.

With the arrival of computer-aided design (CAD), computer-aided engineering (CAE), and computer-aided manufacturing (CAM), there has been a trend towards eliminating the physical models in favour of the virtual models of sculptured parts, which can be designed and machined efficiently by using CAD/CAE/CAM tools. The fields related to efficient design and manufacturing of sculptured parts using CAD/CAE/CAM software packages such as CATIA, Pro/E, ANSYS, and Mastercam, etc. usually include:

- 3D model design of sculptured parts and the part assembly design,
- finite element analysis (FEA) and computational fluid dynamics (CFD),
- multi-axis CNC tool path generation and machining simulation, and
- laser scanning inspection of the finished part surfaces.

CAD/CAE/CAM technology is such a perfect fit that gives users a good solution for the design and manufacturing requirements of sculptured parts. First, 3D solid models with sculptured surfaces can be designed with the CAD tools. For example, a race car with a sculptured body generated in CATIA is shown in Fig. 1.4(a). Then CAE tools are employed to ensure the reliability and the performance of the design of the 3D sculptured parts. For example, the stress analysis of a pair of working gears is realized using the FEA method (see Fig. 1.4(b)). After the design and analysis of the sculptured parts, the tool paths are automatically generated in the CAM module based on the geometric features of sculptured surfaces. The machining process of these parts on multi-axis CNC machine tools can be simulated in the CAM module to verify the tool paths without interference and gouging on the designed surfaces. Fig. 1.4(c) shows a cutter machining the die of a handset along the tool paths in a CNC machining simulation. After the finish

machining of sculptured surfaces, the measurement of the accuracy of these surfaces is quite challenging. The laser scanning tools are commonly used to inspect the finished surface quality. In brief, CAD/CAE/CAM technology sparked off an industrial revolution in the design and manufacturing of sculptured parts. Without this technology, sculptured parts can not be designed with an appealing appearance, analyzed to guarantee required stress and fluid dynamic properties, or manufactured with high efficiency and surface quality.

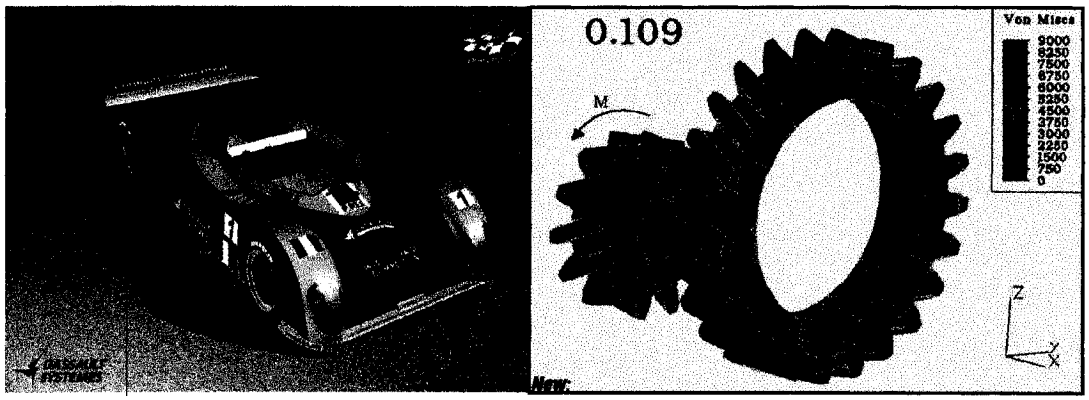

(a) (b)

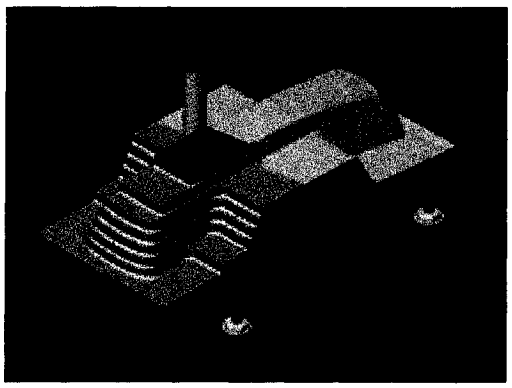

(c)

Figure 1.4 (a) 3D solid model of a race car; (b) stress distribution of a pair of gears; (c) machining simulation of a handset die.

1.3 Three-axis CNC machining of sculptured parts

In general, the machining of a sculptured part on a 3-axis CNC machine mainly consists of five stages: (1) roughing stage, (2) semi-finish stage, (3) finish stage, (4) clean-up stage, and (5) grinding/polishing stage. The roughing stage removes the excess material from the raw stock as quickly as possible. The key features of this stage consist of high

material removal rate (MRR) and rough surface finish, extreme variations in tool-engagement conditions, and constraints of chatter and insert strength [3]. The semi-finish stage obtains a finishing part with a uniform stock allowance. The finish stage forms the final shape of the finished part according to the design with some uncut material. The objective of this stage is to finish the surface machining with adequate-quality surfaces and high productivity concurrently. The key features of the finish stage include long machining time due to small pick-feeds and constraints of tool wear and deflection which affect surface accuracy [3]. The clean-up stage employs small tools to clean the uncut material remained after the finish stage. In the grinding stage, a fine surface is manually polished even without removing any material. Different machining strategies lead to variations in machining efficiency and surface quality. For 3-axis CNC machining, the optimized tool paths can achieve a balance between a shorter machining time and the expected finished surface.

Most sculptured parts are currently machined on three types of CNC machines which are 2½-axis, 3-axis, and 5-axis CNC machines. According to the different features of the rough and finish stages, 2½-axis CNC machines are normally used for the rough machining, and the 3-axis and 5-axis CNC machines are usually used for the finish machining of sculptured parts. The cutters on these machines are classified into three common types: ball, torus, and flat end-mill (see Fig. 1.5). Among these CNC machines, the 3-axis milling machine is a typical CNC machine. By use of mechanical automated motors, the working table moves along the X axis and the Y axis, while the cutter moves along the Z axis simultaneously. There are two types of 3-axis CNC milling machines: horizontal and vertical. The main feature of both machines is that the cutter orientation

with respect to the machining part is locked after the part is fixed on the worktable. A 3-axis CNC vertical milling machine is shown in Fig. 1.6; the cutter orientation is always in the vertical direction.

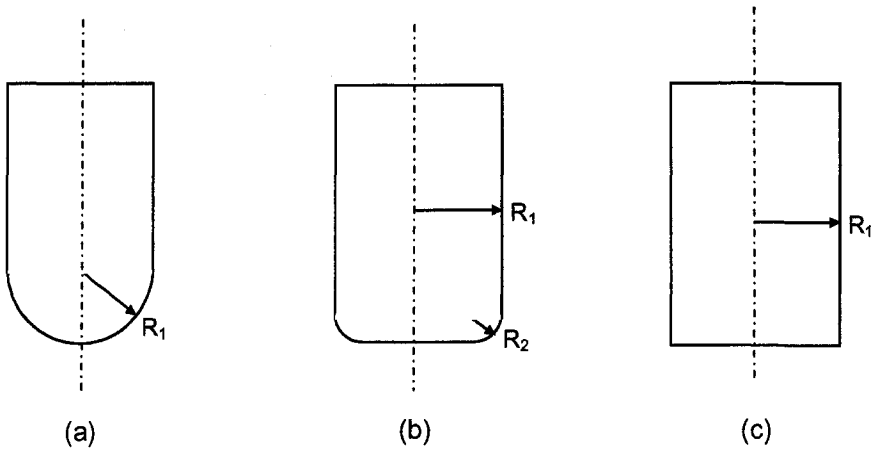

Figure 1.5 Three types of common milling cutters. (a) Ball end-mill; (b) torus end-mill; (c) flat end-mill.

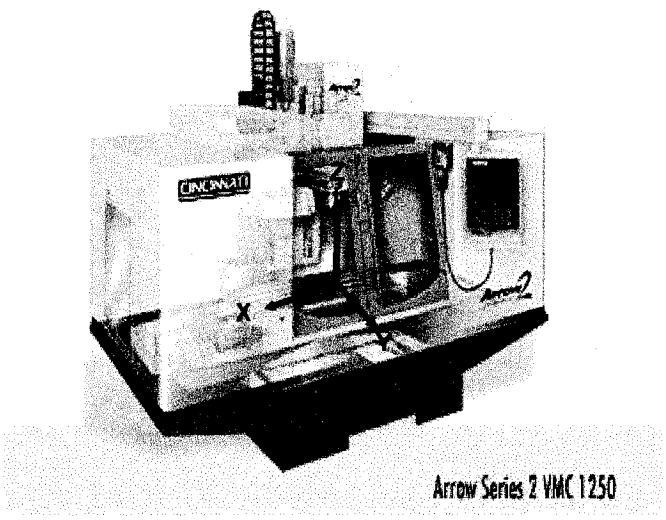

Figure 1.6 Diagram of a 3-axis CNC vertical milling machine.

Although three-axis CNC machining is not a universal solution for the milling of all types of sculptured surfaces, it is still the most popular one in the manufacturing industry. Statistics show that the majority of sculptured parts in the die/mold industry are made with the 3-axis CNC machine tools. The reason for this is that the 3-axis CNC machining has some advantages compared with 5-axis CNC machining. First of all, the machine is affordable even for small businesses and its maintenance is not expensive. Secondly, higher stiffness and rigidity of the machine prevents chatter in machining. Moreover, programming for tool paths in 3-axis CNC machining is manageable. Finally, machine accuracy is high enough to meet the requirements of finishing machining. Therefore, 3-axis CNC machining is a major force in the manufacturing industry of sculptured parts. The machining errors occurred in the machining directly determine the finish surface quality of sculptured parts.

1.4 Machining-error predictions for three-axis CNC milling of sculptured parts

In 3-axis CNC machining, machining errors are usually caused by some of the sources such as cutting tool deflection, cutting tool wear, machine tool vibration, improper coolant/lubrication, and negative thermal effect. To improve part accuracy, many approaches have been proposed to predict cutting forces and machining errors in different cutting conditions. Lim et al. [4, 5] evaluated the instantaneous horizontal cutting-forces at cutter contact (CC) points based on the un-deformed chip geometry and calculated the horizontal tool deflections to determine the machining errors. Feng and Menq [6] presented a flexible system model that utilizes both instantaneous and regenerative

feedbacks of the deflections in the cutting system for more precise representation of the chip geometry in order to accurately predict cutting forces and machining errors in ball end milling. Yun et al. [7] proposed a new method that predicts the errors on the machined surface during peripheral end milling. Ikua et al. [8] investigated the influence of various cutting conditions, styles, and modes on the cutting forces and machining errors in ball end milling of cylinder surfaces. These studies have been conducted based on simply-shaped parts with good geometric matching to the cutting tools.

However, for sculptured surfaces that are more complex in shape, the geometry of a cutting tool does not well match a free-form surface if the tool cuts along tool paths in a point-to-point way. As a consequence, this tool-surface mismatch is deemed to cause the inaccuracy of the machined surfaces, even if there is no other source of error in ideal machining conditions. Sometimes, the machining error caused by tool paths is serious, resulting in surface gouging. To predict the maximum machining error in a tool step, a popular, approximate way - the chordal deviation method - is to calculate the maximum distance between the tool path and the chord connecting the two CC points of this step [9, 10]. Choi et al. [3] presented the circular arc approximation method for computing machining errors based on two assumptions: (a) the tool path between two CC points is roughly fit with a circular arc, and (b) the surface normals at the CC points are estimated with those of the circular arc. The limitation of these two established methods is that their predictions are not accurate enough for sculptured surface machining.

When a tool cuts from one CC point to the next, the tool sweeps a 3D volume; and the bottom part of the boundary surface of this volume is called the cutter-swept surface.

From the geometry point of view, all the stock material enclosed in a cutter-swept surface can be removed; so the portion of this surface that is inside the part surface represents the geometry of the furrow formed on the machined surface. Wang and Wang [11] used a numerical model for the volume swept by a tool moving along a tool path. Altintas and Spence [12] modeled the workpieces and swept volumes along the tool paths using solid primitives and Boolean operations. Blackmore et al. [13] used a boundary flow formula and a sweep-envelope differential equation as the theoretical framework to construct the swept volumes of a tool. Chung et al. [14] constructed a closed-form equation for the cutter-swept surfaces in 3-axis NC machining. Roth et al. [15] generated a cutter-swept surface for a torus end-mill by calculating a group of points on the donut-shaped cutting surface as the 3D silhouette curve and sweeping these points along the tool feed direction. Similarly, Chiou and Lee [16] derived a parametric representation of swept profiles for an APT cutter in 5-axis CNC machining. These methods can be used in machining simulations; however, they are either very difficult to implement or limited to certain types of cutting tools. None of them has been applied directly to predict machining errors. If the machining errors are predicted accurately, a number of CC points along tool paths can be determined properly with respect to the specified tolerance.

1.5 Cutter contact point determination in three-axis CNC milling of sculptured parts

Sculptured surface milling on the 3-axis CNC machine is mostly regarded as solving a geometric problem between a part surface and a tool cutter. Due to the diversity and complexity of geometric relations between a free-form surface and a tool cutter, it has

remained a major technical challenge to achieve high surface quality and productivity. Consequently, well-planned CNC tool paths which come beforehand, corresponding to the designed surface are crucial to surface quality and machining time in the machining of the sculptured surfaces. Research on tool path planning includes tool path pattern selection, and cross-feed (or tool path interval) and step length (or cutter contact points) determination. Many approaches have been proposed to choose the tool path patterns such as iso-parametric [17 - 19], parallel planar [20], iso-cusped [21 - 23], steepest-ascending [24], and integrated steepest-ascending and iso-cusped [25] tool path planning methods. Due to the geometric complexity of the sculptured surfaces, the cutting tool does not match the surfaces. Thus the tool is deemed to cause errors when it passes through the cutter contact (CC) points along a line segment in machining. However, little research has been conducted on the CC points (or step length) determination.

To prevent sculptured surfaces from being gouged where the machining error is larger than the tolerance, state-of-the-art CAM software usually determines CC points on the tool paths, and simulates the machining to detect gouging [26]. If gouging is found, the CC points have to be re-determined in another loop. As a consequence, the CC points cannot be optimized in this way. Besides, the software accuracy is usually limited up to 0.01 *mm*, and hence the validity of the gouging detection is not ensured if a part tolerance is less than 0.01 *mm*. Thus the limitations of this established method are that it is time-consuming and sometimes ineffective. To determine the step length for each tool motion, a conservative way [18] is to take a constant, very small step length along a tool path, resulting in a huge number of CC points. Unfortunately, this method causes longer machining time, poor machine-tool dynamics, and unnecessarily large CNC programs. In

particular, if the tool paths are iso-parametric curves, several researchers have suggested a conservative, constant increment of the varying parameter as the step length to determine the CC points [27]. Due to the nonlinear mapping from the parametric space to the 3D Cartesian space, the overall surface accuracy and finish is not consistent, sacrificing the surface quality.

In tool path planning for sculptured surfaces, one objective is to optimize step length according to the tool path geometry, so that each tool step is as long as possible and all machining errors in each step are within the specified tolerance [17]. In other words, the number of CC points should be minimized, and surface accuracy still meets the tolerance requirement. Some research [27] took the curvatures of the tool paths into account and predicted the maximum machining error in a tool step using the maximum distance between the tool path and the chord connecting the two CC points of the tool step. By adjusting the CC points, the step length is changed and the maximum machining error meets the specified tolerance. Choi and Jerard [17] and George and Ramesh [18] improved the technique of predicting the maximum machining error and calculated the CC points for accurate machining of analytical surfaces such as cylinders and spheres. However, it could not be used to optimize CC points for complex free-form surfaces.

1.6 Objectives of this thesis

Since none of the established methods is able to accurately predict the machining error in a tool step caused by the tool-surface mismatch, the step length between the two CC points can not be maximized to meet the specified tolerance. In other words, there has

been no appropriate system provided to optimize the number of CC points along tool paths.

Therefore, the objectives of this thesis research work include:

- propose a generic, geometric approach to predicting machining-error accurately for 3-axis CNC milling of sculptured surface parts; and
- propose a cutter contact point optimization system to implement this new approach.

1.7 Outline of this thesis

This thesis is divided into four chapters. Chapter one introduces sculptured parts, CAD/CAE/CAM of these parts, 3-axis CNC machining of these parts, and machining errors occurring in the 3-axis CNC machining. Having introduced the problems of the prediction of the machining errors, the determination of CC points is further discussed in this chapter. Chapter two provides the geometric model of furrows of machined surfaces. Machining errors are predicted accurately based on the model. Then an approach to accurate machining-error predictions is provided. In chapter three, different methods of machining-error predictions are described. A CC point optimization system is proposed to implement this new approach. Applications and analysis are imposed to show its feasibility. At last, a summary and the contributions of this thesis research are provided.

Chapter 2 Cutter-Swept Surface Modeling and Formulation

In this chapter, a generic, geometric approach to predicting accurate machining errors due to the tool-surface mismatch is proposed for 3-axis CNC milling of sculptured surfaces. First, a new geometric model of the furrow formed by an APT milling tool moving between two neighbouring CC points is built. Second, a mathematical formula of the cutting circle envelopes is derived. Then an algorithm of calculating machining errors in each tool motion is provided. Finally, this new approach is applied to two practical parts for the accurate machining-error predictions, and these predictions are then compared to the inaccurate predictions made by two established methods to demonstrate the advantages of this approach.

2.1 Geometric model of furrow patches of machined surfaces

In the 3-axis milling of a sculptured surface, when the tool passes through CC points along the tool paths planned for this surface, all furrows of the machined surface are formed in the tool motions. Since the tool cannot exactly match it in shape, the sculptured surface is machined with errors. Here, the machining error at a surface point is the shortest distance between this point and its corresponding furrow, and the surface

accuracy is defined as the maximum of the machining errors at all points across the surface. Contrary to the conventional notion, this tool-surface mismatch in fact is a dominant cause of errors in surface milling; thus to accurately predict this type of machining errors, this research study builds a generic, geometric model of furrow patches.

2.1.1 Geometric model of furrow patches machined using flat end-mills

The furrows are determined by the geometry of the cutting tool and the surface, as well as the tool paths. Usually a furrow consists of many furrow patches, one between two adjacent CC points. To establish the geometric model, the mechanism of removing excess stock material in a tool motion should be clearly understood. First, the geometry of a tool can be regarded as a family of thin disks piled along the tool axis, and all the disks have the same number of cutting edges as the tool. Since the cutting speed is usually much larger than the feed rate during machining, the trochoidal trajectory of each cutting edge tip can be approximated as a circle [4 - 6]. Thus in this thesis research work the tool's working surface during machining is regarded as many cutting circles, which are illustrated on a general APT milling tool and three typical end-mills in Fig. 2.1. The following is the introductory analysis of the material removing mechanism in a flat end milling.

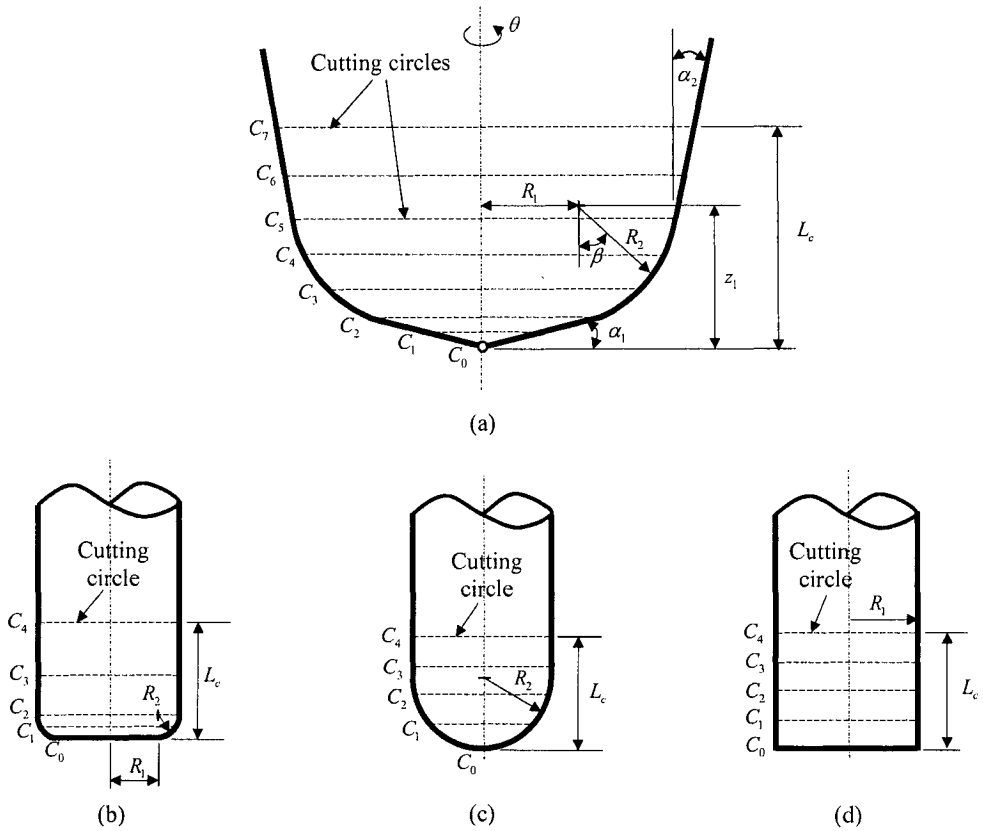

Figure 2.1 (a) APT tool; (b) torus end-mill ($\alpha = 0$ and $\beta = 0$); (c) ball end-mill ($\alpha = 0$, $\beta = 0$, and $R_1 = 0$); (d) flat end-mill ($\alpha = 0$, $\beta = 0$, and $R_2 = 0$).

Suppose a flat end-mill is cutting a sculptured surface S between two CC points CC_1 and CC_2 on a 3-axis vertical CNC milling machine (see Fig. 2.2). At the location CL_1, the tool is cutting the surface at point CC_1, where the bottom cutting circle C_0 is tangent to the surface. The stock material inside the cutting circles C_0 to C_5 is removed. The tool then moves to the cutter location CL_2 along the tool feed direction. Since the cutting circles moves simultaneously with the tool, the material on any layer between the CC points is gradually removed by the cutting circles

between the layer and the bottom cutting circle after they reach the layer one by one. For instance, the cutting circle C_5 removes the material on a layer at a height of z when the cutter machines at CC_1. Then C_4 reaches the layer and cuts. Similarly, all the cutting circles C_3, C_2, C_1, and C_0 arrive sequentially and remove the stock material left by its previous cutting circle (hatched with different patterns in Fig. 2.2). Hence the profile of all the removed material can be formulated as the envelope of the cutting circles, and on the layer the shape of the furrow can be represented as the portion of the profile inside the surface.

The machining mechanism occurs on each layer, and the furrow patch is formed until the cutter finishes the tool motion at CL_2. In this research work, the geometry of the furrow patch is modeled layer by layer (see Fig. 2.2) to represent the final surface shape cut inside the surface and between the CC points.

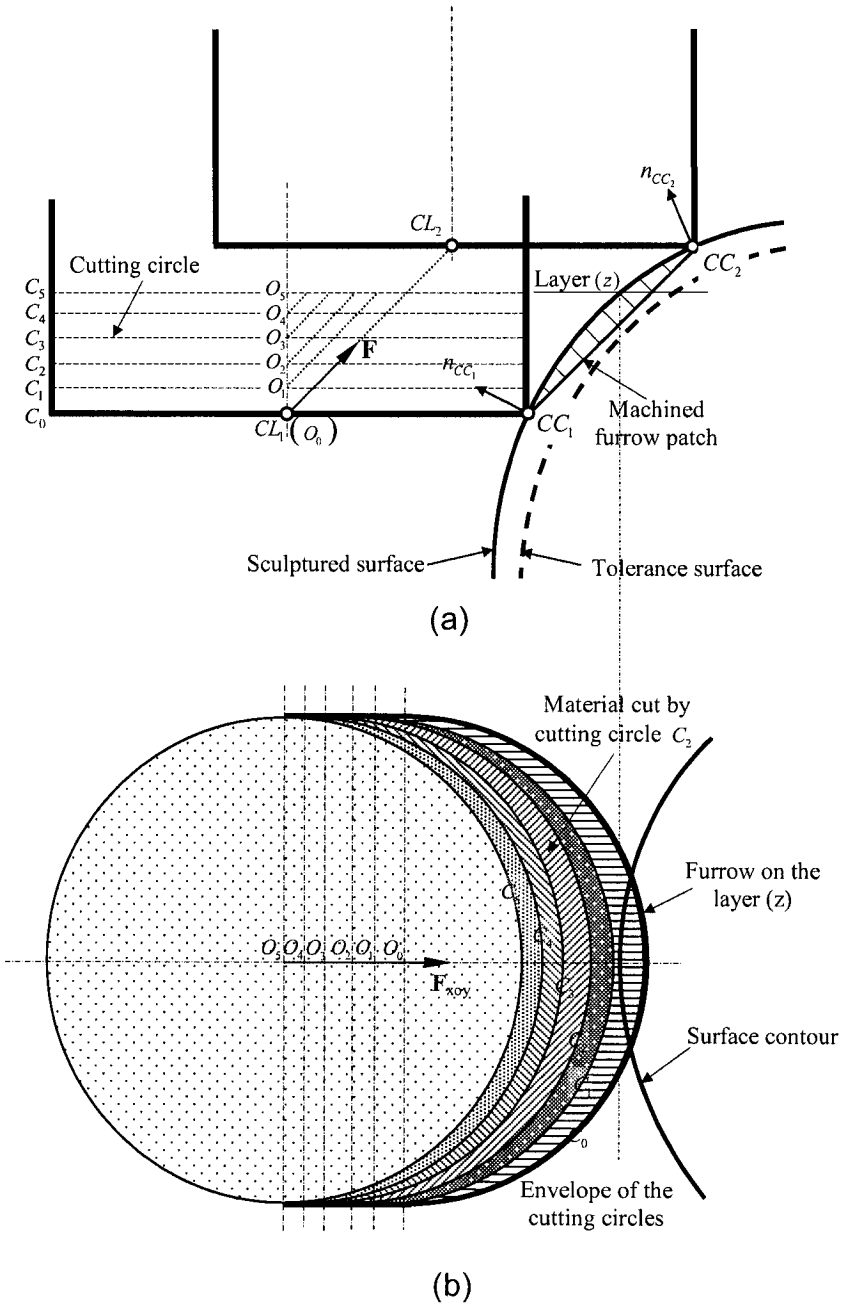

Figure 2.2 Geometric model of furrow patches. (a) A flat end-mill step in surface milling; (b) the envelope of the cutting circles on layer (z).

2.1.2 Geometric model of furrow patches machined using APT tools

Based on the previous analysis, the machining mechanism of any type of milling tools can be found, and the geometric model of furrow patches can be established. Since the cutting surfaces of all available milling tools are different, the shapes of the furrow patches machined with these tools are different. It is necessary to work on the generic milling tool, the APT tool, for its machining mechanism, which can be applied to any specific milling tools (see Fig. 2.1).

Suppose an APT tool cuts a surface between two CC points CC_1 and CC_2 along a tool feed direction on a vertical 3-axis CNC machine (see Fig. 2.3). The cutter locations of CC_1 and CC_2 are CL_1 and CL_2, respectively, and the tool feed direction (**F**) is a vector from CL_1 to CL_2. The cutting surface of the cutter is regarded as a family of cutting circles perpendicular to the tool axis, and some of them $C_0, C_1, C_2, ..., C_{10}$ are shown in Fig. 2.3. Among these cutting circles, C_t passes through the point at which the tool feed direction (**F**) is tangent to the cutting surface. In this motion, the cutting circles rotate and move simultaneously along the same tool feed direction to remove the stock material. To understand the machining mechanism, the process of removing the stock material is closely examined.

First, make a horizontal plane Ω passing through the CC point CC_1. At beginning, the tool is located at CL_1 and tangent to the surface at CC_1. A cutting circle C_{CC_1} is tangent to the surface at CC_1. All the cutting circles remove the stock material inside them, and the cutting circle C_{CC_1} removes the stock material on the

plane Ω and inside the circle. As the tool moves along the tool feed direction, the cutting circle C_{CC_1} leaves the plane Ω, and a cutting circle beneath C_{CC_1} reaches and cuts on the plane. For example, the cutting circle C_5 moves along the tool feed direction and relocates on Ω at $O_{5,\Omega}$, which is denoted as $C_{5,\Omega}$, and removes the stock material between C_{CC_1} and $C_{5,\Omega}$. Then the cutting circles C_4 comes in and is centered at $O_{4,\Omega}$. The material between $C_{5,\Omega}$ and $C_{4,\Omega}$ is cut. Until the cutting circle C_t reaches Ω at $O_{t,\Omega}$, the process of removing the material on Ω is finished, and the cutting circles between C_t and C_0 do not remove any material when they reach on the plane Ω (see Fig. 2.3). Thus all the stock material on Ω and inside the family of the cutting circles C_{CC_1}, $C_{5,\Omega}$, $C_{4,\Omega}$, and $C_{t,\Omega}$ is removed, and the profile of the family of these cutting circles is the envelope of the cutting circle. The part of the profile inside the surface contour on Ω is the shape of the furrow on that plane. Since the CC point CC_1 is inside the profile, it is removed in machining. However, a common notion about surface milling is that all CC points are machined and remained on the machined surface, which is not true for many milling tools.

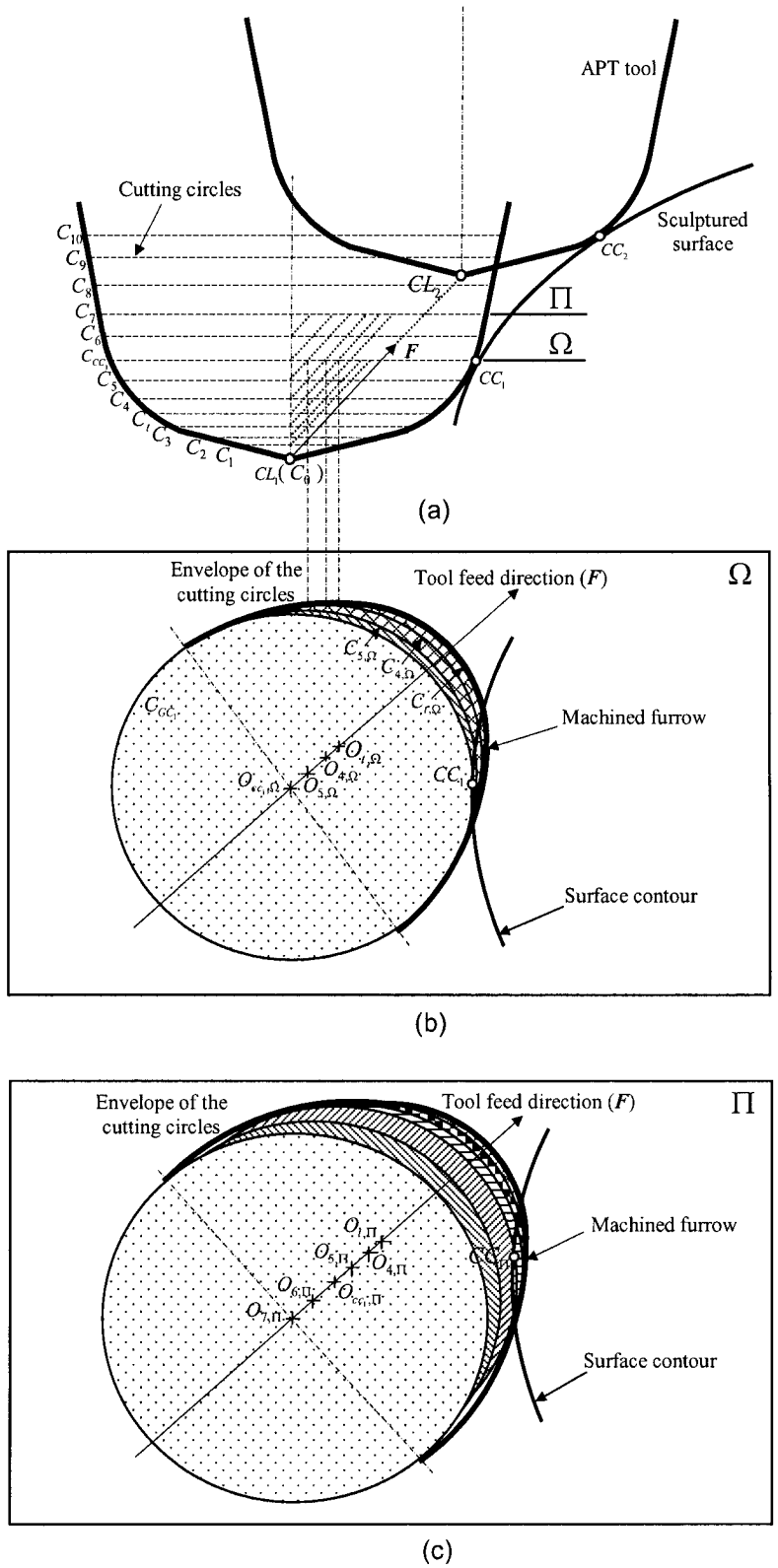

Figure 2.3 Geometric model of furrow patches. (a) An APT tool step; (b) the envelope of cutting circles on layer Ω; (c) the envelope of cutting circles on layer Π.

A similar machining process occurs at different places in the course of the tool motion. Suppose a horizontal layer Π is between CC_1 and CC_2 as shown in Fig. 2.3, and it intersects with the tool at cutting circle C_7. In machining, the cutting circles below C_7 reach on Π consecutively. The cutting circles, C_6, C_{cc_1}, C_5, C_4, C_3, and C_t, cut the material in sequence after they approach Π in the tool feed direction, and then leave Π in the same direction one by one. The profile of these cutting circles can represent the machined shape of the part on the layer after this tool motion. Since the furrow patch is inside the surface, the shape of the furrow on Π is determined by a portion of the profile that is inside the surface contour on Π.

Therefore, the geometric model of a furrow patch between two CC points can be built layer by layer. On each layer, first find the profile of the cutting circles between this layer and C_t, and then calculate the surface contour on the layer. The part of the profile inside the surface contour is the shape of the furrow patch on the layer. This geometric model is easy to implement and is effective for either upward or downward milling of convex and concave surfaces. It is a generic model for any type of milling tools used in machining. It can be used in machining simulation as well.

2.2 Envelope of cutting circles

To establish the geometric model of a furrow patch between two adjacent CC points, the profile of the family of cutting circles should be formulated. Since the profile is the envelope of these circles, the closed form equation of the envelope can be derived. An

APT tool is used in order to find the generic formula of the envelope, which can be applied to any type of milling tools.

Suppose on a 3-axis vertical CNC milling machine, an APT tool (see Fig. 2.1 for dimensions) cuts a part surface S from a CC point $CC_1 = [CCx_{1,p}, CCy_{1,p}, CCz_{1,p}]$ to another $CC_2 = [CCx_{2,p}, CCy_{2,p}, CCz_{2,p}]$ in the part coordinate system (X_p, Y_p, Z_p) (see Fig. 2.4). The surface normal $\mathbf{n}_{CC_1,p} = [nx_{1,p}, ny_{1,p}, nz_{1,p}]^T$ at point CC_1 and its cutter location $CL_1 = [CLx_{1,p}, CLy_{1,p}, CLz_{1,p}]^T$ can be calculated using the following equation.

$$\begin{cases} CLx_{CC_1,p} = CCx_{1,p} + R_2 \cdot nx_{1,p} + \frac{nx_{1,p}}{\sqrt{nx_{1,p}^2 + ny_{1,p}^2}} \cdot R_1 \\ CLy_{CC_1,p} = CCy_{1,p} + R_2 \cdot ny_{1,p} + \frac{ny_{1,p}}{\sqrt{nx_{1,p}^2 + ny_{1,p}^2}} \cdot R_1 \\ CLz_{CC_1,p} = CCz_{1,p} + R_2 \cdot nz_{1,p} - z_1 \end{cases} \tag{2.1}$$

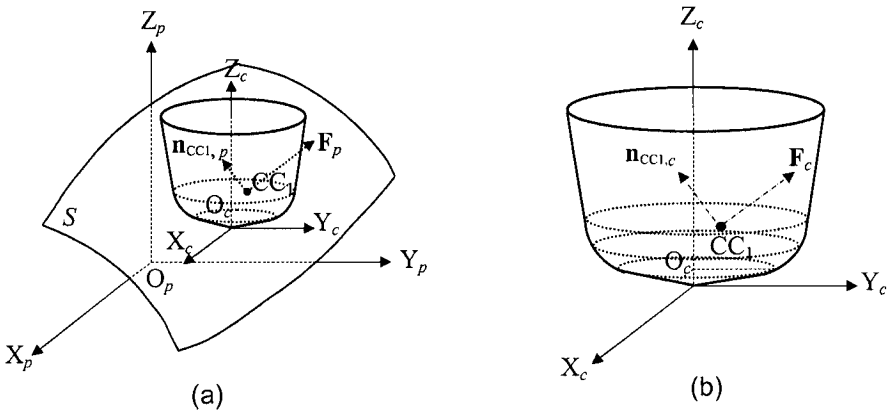

Figure 2.4 APT tool in the part and cutter coordinate systems.

Similarly, the surface normal $\mathbf{n}_{CC_2,p} = [nx_{2,p}, ny_{2,p}, nz_{2,p}]^T$ at point CC_2 and its cutter location $CL_2 = [CLx_{2,p}, CLy_{2,p}, CLz_{2,p}]^T$ can be calculated. The tool feed direction $\mathbf{F}_p = [Fx_p, Fy_p, Fz_p]^T$ is calculated and represented in the part coordinate system.

To derive the equation of the envelope, a cutter coordinate system (X_c, Y_c, Z_c) is built by translating the part coordinate system from O_P to O_c (see Fig. 2.4). The transformation matrix from the part coordinate system to the cutter coordinate system is

$$[T] = \begin{bmatrix} 1 & 0 & 0 & -CLx_{1,p} \\ 0 & 1 & 0 & -CLy_{1,p} \\ 0 & 0 & 1 & -CLz_{1,p} \\ 0 & 0 & 0 & 1 \end{bmatrix} \tag{2.2}$$

Using the above transformation matrix, the coordinates of CC_1 and CC_2, the surface normals at the two points, and the tool feed direction in the part coordinate system are transformed into the cutter coordinate system as $CC_1 = [CCx_{1,c}, CCy_{1,c}, CCz_{1,c}]$, $CC_2 = [CCx_{2,c}, CCy_{2,c}, CCz_{2,c}]$, $\mathbf{n}_{CC_1,c} = [nx_{1,c}, ny_{1,c}, nz_{1,c}]^T$, $\mathbf{n}_{CC_2,c} = [nx_{2,c}, ny_{2,c}, nz_{2,c}]^T$ and $\mathbf{F}_c = [Fx_c, Fy_c, Fz_c]^T$, respectively.

To find the generic equation of the envelope of the cutting circles, the layer Π in the above section is adopted here. Assume the z coordinate of Π in the cutter coordinate system is z_Π, and $z_\Pi > z_1 - R_2 \cdot \sin\alpha_2$ (see Fig. 2.5). The cutting circles that are on the upper conic cutting surface and below Π are represented as

$$\begin{cases} x = \left[R_1 + \dfrac{R_2 + (z - z_1)\cdot \sin\alpha_2}{\cos\alpha_2} \right] \cdot \cos\theta \\ y = \left[R_1 + \dfrac{R_2 + (z - z_1)\cdot \sin\alpha_2}{\cos\alpha_2} \right] \cdot \sin\theta \end{cases} \qquad (0 \le \theta \le 2\cdot\pi) \tag{2.3}$$

For a practical $\mathbf{F}_c$, the cutting circle C_t should be on the toroidal cutting surface. The z coordinate of C_t in the cutter coordinate system can be calculated as

$$z_{C_t} = R_1 + R_2 \cdot (1 - \sin\beta_{C_t}) \text{ and } \beta_{C_t} = \arccos\left(\frac{Fz_c}{\sqrt{Fx_c^2 + Fy_c^2 + Fz_c^2}}\right) \tag{2.4}$$

For all cutting circles on the toroidal cutting surface and above C_t, their z coordinates change in an interval $[z_1 - R_2 \cdot \sin\alpha_2,\ z_{C_t}]$, and each z corresponds to a cutting circle. Based on the z value of each of the cutting circles C_i, its center O_i is $(0,0,z)$ in the cutter coordinate system, and its radius can be found as $R_1 - R_2 + \sqrt{2\cdot R_2 \cdot z - z^2}$.

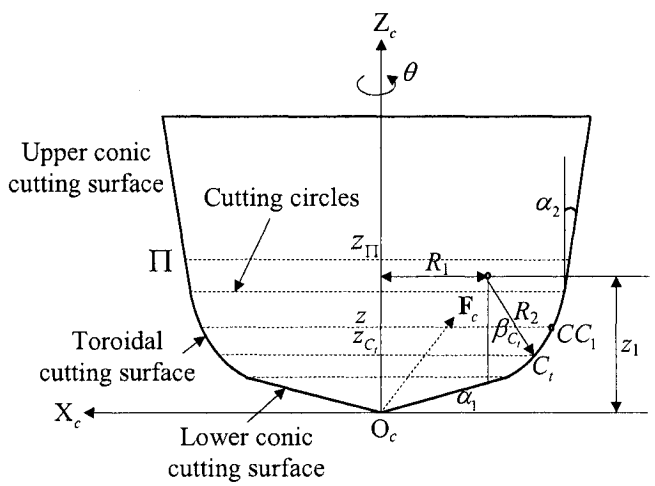

Figure 2.5 Cutting circles in different cutting surfaces in the cutter coordinate system.

When the cutter moves along $\mathbf{F}_c$, the cutting circles C_i reach Π in sequence, and their centers are relocated on Π. The center (x, y) of C_i on Π can be calculated as

$$\begin{cases} x = \frac{Fx_c}{Fz_c} \cdot (z_\Pi - z) \\ y = \frac{Fy_c}{Fz_c} \cdot (z_\Pi - z) \end{cases} \tag{2.5}$$

Therefore, the equation of the cutting circle on Π moved from the upper conic cutting surface C_i is

$$\begin{cases} x = \frac{Fx_c}{Fz_c} \cdot (z_\Pi - z) + \left[R_1 + \frac{R_2 + (z - z_1) \cdot \sin\alpha_2}{\cos\alpha_2} \right] \cdot \cos\theta \\ y = \frac{Fy_c}{Fz_c} \cdot (z_\Pi - z) + \left[R_1 + \frac{R_2 + (z - z_1) \cdot \sin\alpha_2}{\cos\alpha_2} \right] \cdot \sin\theta \qquad (0 \le \theta \le 2 \cdot \pi) \\ z = z_\Pi \end{cases} \tag{2.6}$$

The equation of the cutting circle on Π moved from the toroidal cutting surface is

$$\begin{cases} x = \frac{Fx_c}{Fz_c} \cdot (z_\Pi - z) + \left[R_1 - R_2 + \sqrt{2 \cdot R_2 \cdot z - z^2} \right] \cdot \cos\theta \\ y = \frac{Fy_c}{Fz_c} \cdot (z_\Pi - z) + \left[R_1 - R_2 + \sqrt{2 \cdot R_2 \cdot z - z^2} \right] \cdot \sin\theta \qquad (0 \le \theta \le 2 \cdot \pi) \\ z = z_\Pi \end{cases} \tag{2.7}$$

where θ is the parameter of C_i. When z varies in an interval $[z_{C_i}, z_\Pi]$, Eq. 2.6 or 2.7 represents one of the family of the cutting circles relocated on Π. The envelope E of these cutting circles must meet the equation as

$$\frac{\partial x}{\partial z}\cdot\frac{\partial y}{\partial \theta}-\frac{\partial x}{\partial \theta}\cdot\frac{\partial y}{\partial z}=0 \tag{2.8}$$

By solving the equation (2.7), the relationship between variables z and θ can be found. So for the cutting circles on the upper conic cutting surface, their z components meet $z_{\Pi} > z > z_1 - R_2 \cdot \sin\alpha_2$, and the envelope E_1 on Π formed by these cutting circles can be found with the following equation in the cutter coordinate system.

$$\begin{cases} x = \frac{Fx_c}{Fz_c}\cdot(z_{\Pi}-z)+\left[R_1+\dfrac{R_2+(z-z_1)\cdot\sin\alpha_2}{\cos\alpha_2}\right]\cdot\cos\theta \\ y = \frac{Fy_c}{Fz_c}\cdot(z_{\Pi}-z)+\left[R_1+\dfrac{R_2+(z-z_1)\cdot\sin\alpha_2}{\cos\alpha_2}\right]\cdot\sin\theta \\ \theta = \gamma \pm \arccos(\tan\alpha_2) \end{cases} \tag{2.9}$$

Similarly, for the cutting circles on the toroidal cutting surface, their z coordinates meet $z_1 - R_2 \cdot \sin\alpha_2 > z > z_1 - R_2 \cdot \cos\alpha_1$, the envelope E_2 on Π formed by can be found as well.

$$\begin{cases} x = \frac{Fx_c}{Fz_c}\cdot(z_{\Pi}-z)+(R_1-R_2+\sqrt{2\cdot R_2\cdot z-z^2})\cdot\cos\theta \\ y = \frac{Fy_c}{Fz_c}\cdot(z_{\Pi}-z)+(R_1-R_2+\sqrt{2\cdot R_2\cdot z-z^2})\cdot\sin\theta \\ \theta = \gamma \pm \arccos(\frac{Fz_c}{\sqrt{Fx_c^2+Fy_c^2}}\cdot\frac{R_2-z}{\sqrt{2\cdot R_2\cdot z-z^2}}) \end{cases} \tag{2.10}$$

where γ is calculated in two conditions. If $Fy_c > 0$, $\gamma = \arccos(\dfrac{Fx_c}{\sqrt{Fx_c^2+Fy_c^2}})$; and if $Fy_c < 0$, $\gamma = 2\cdot\pi - \arccos(\dfrac{Fx_c}{\sqrt{Fx_c^2+Fy_c^2}})$.

The generic formulas of the envelope include all the cases on the layers. Depending on the height of a layer, Eq. 2.9 and 2.10 can be used to calculate the envelope on that layer. In a special case when the tool feed direction is horizontal or the tool machines a plane, the profile of all three cutting surfaces along **F** is shown in Fig. 2.1 and the equations of the envelope cannot be applied. However, this is the simplest case and can be solved directly.

Based on the generic formulas, the envelope on each layer can be found. Since the surface contour is easy to get on each layer, the intersection points between the two curves can be found, and the portion of the envelope that is inside the contour is determined as the shape profile of the furrow on the layer (see Fig. 2.3). All the shape profiles are lined up along the tool feed direction forming a furrow patch. A property of the furrow patch is the projection of this patch onto a plane perpendicular to the tool feed direction is a curve on this plane. With the help of this property, the calculation of the machining errors can be simplified. The generic formulas can be applied to different types of cutting tools, such as ball, bull nose, or flat end-mills.

2.3 Machining-error predictions

Based on the geometric model of furrow patches, a furrow patch can be computed if two adjacent CC points are chosen on a tool path. Thus the machining error at a point on the local surface area between the two CC points can be predicted accurately.

To find the machining accuracy of a local surface area between two adjacent CC points, first, choose a proper number of horizontal layers between the CC points, and

calculate the surface contour and the envelope of cutting circles on each layer (see Fig. 2.6(a)). Second, find the two intersection points between the surface contour and the envelope and take a number of sample points on the surface contour and between the intersection points (see Fig. 2.6(b)). Third, project the sample points and the envelope onto a plane perpendicular to the tool feed direction and compute the minimum distances on the plane between the projections of the sample points and the envelope as the machining errors at the sample points (see Fig. 2.6(c)). Then locate the maximum of all machining errors at the sample points. This procedure is applied to all the layers for maximum machining errors. Finally, find the overall maximum machining error of all the selected layers as the machining accuracy of the local surface area.

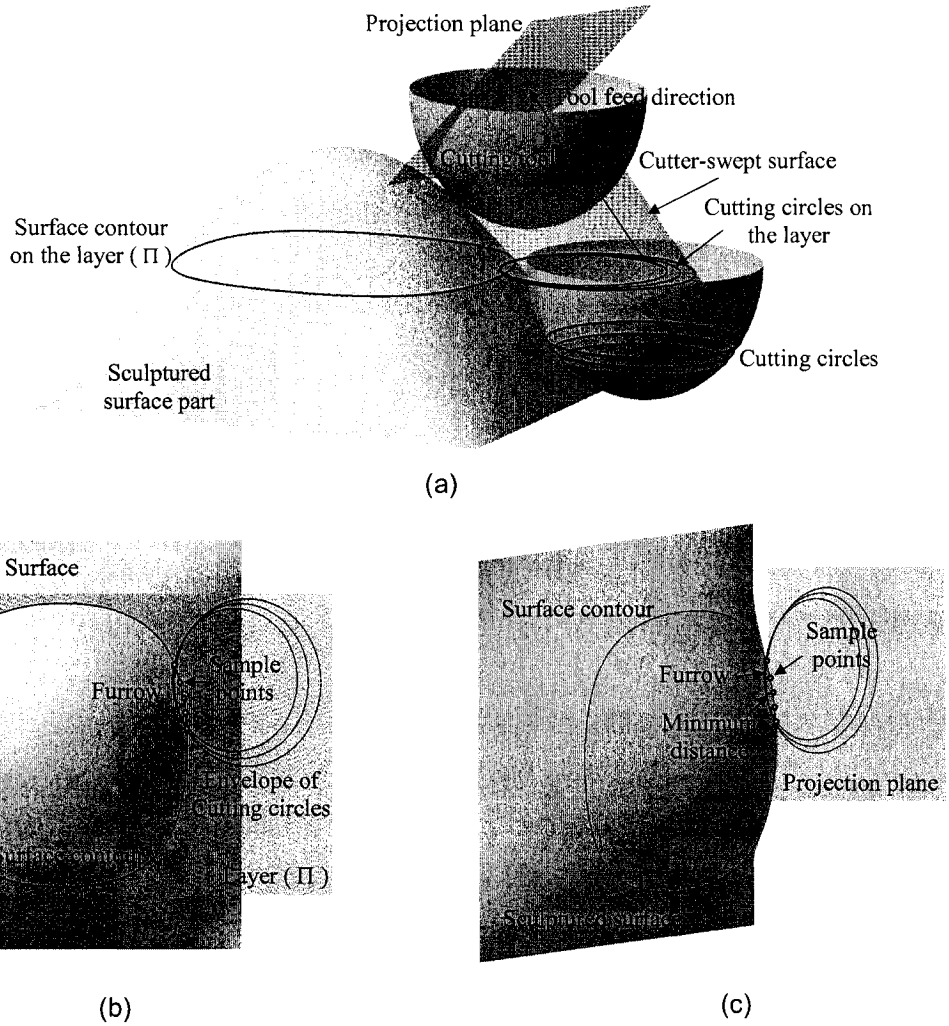

Figure 2.6 Illustration of machining-error predictions. (a) Cutter-swept surface between two CC points; (b) surface contour and an envelope of cutting circles on a layer; (c) projection of the envelope and the surface contour.

This approach is accurate and effective to predict machining errors by tool paths because this complex 3D problem is simplified and solved in a 2D way. The number of horizontal layers and sample points on each surface contour is adjustable. The machining error at a surface point is the minimum distance between the point and the machined surface. The main application of this approach is to optimize CC points on tool paths of

sculptured surfaces. When the optimized CC points are used with G1 function in CNC milling machines, the part surface is free of gouging. This approach can also be used in machining simulation to facilitate representing the geometry of machined surfaces.

2.4 Examples

To demonstrate its feasibility and advantages, this proposed approach has been implemented in a software system for predicting machining errors accurately. This system is used to calculate the machining errors for a regular semi-cylindrical surface part (see Fig. 2.7) and a NURBS surface part (see Fig. 2.9). Meanwhile, two established approximation methods, the chordal deviation method [9, 10] and the circular arc approximation method [3], are also applied to the same parts for predicting the machining errors. The results are then compared to show the fidelity of these approximation methods.

Specifically, for the semi-cylindrical part with a radius of 25.4 *mm* and a length of 50.8 *mm* shown in Fig. 2.7, six tool paths (1 to 6) are generated by a series of planes cutting through the part at different inclination angles α such as 90°, 75°, 60°, 45°, 30°, and 20°, respectively (see Fig. 2.8(a)). A ball end-mill with a radius of 12.7 *mm* is used, and the surface tolerance is 0.1 *mm*. On each tool path, a pair of CC points is selected such as A_1A_2 on tool path 1 or D_1D_2 on tool path 4. This proposed approach is applied to calculate the furrow patch between each pair of CC points, and the patch between D_1 and D_2 is depicted in Fig. 2.8(b) for its details. All furrow patches of the machined surface can be found by applying this approach to each tool motion.

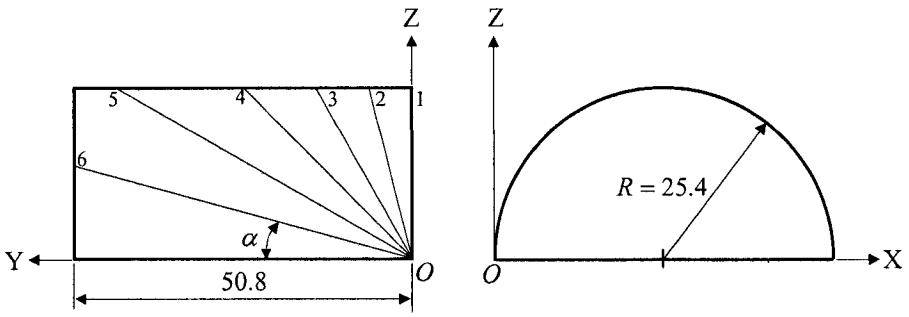

Figure 2.7 Six tool paths on a regular semi-cylindrical surface part.

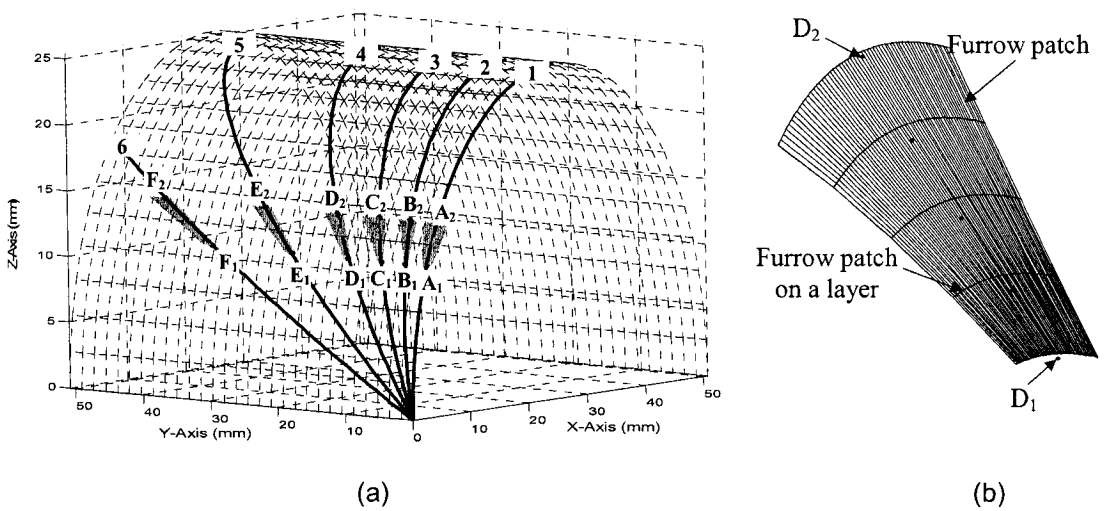

Figure 2.8 Furrow patch between two CC points on the semi-cylindrical surface part.

To compare the two established approximation methods with this proposed approach, these three methods are employed to calculate the maximum machining errors of the local surface areas between the selected CC points. As shown in Table 1, for the maximum machining error between A_1 and A_2, the prediction of the circular arc approximation method is the same as the accurate result (0.1 *mm*) of this proposed approach;; but the chordal deviation method predicts the machining error as 0.0667 *mm*,

which is under-estimated by 33%. From path 1 to 6, the predicted machining errors of the circular arc approximation method become smaller, compared to those of this proposed approach; thus these machining errors are also under-estimated, and the prediction accuracy is decreased. For example, the maximum machining error between F_1 and F_2 on path 6 is calculated as 0.0709 *mm*, which is least accurate; unfortunately, the prediction accuracy drops 30%.

Unlike the circular arc approximation method, using the chordal deviation method to predict the maximum machining error, the result is getting better from path 1 to 6. However, the discrepancy between the approximate prediction and the accurate prediction always remains high, so the prediction accuracy is low. Between F_1 and F_2 on the tool path 6, the machining error is under-estimated as 0.0713 *mm*, which is 40% off the accurate prediction of this proposed approach. Therefore, the fidelity of these established methods is challenged in machining-error predictions.

Table 2.1 Predicted maximum machining errors in the selected tool steps by the three methods

Unit: *mm*	Machining tolerance: 0.1 *mm*	Ball end-mill: $D = 25.4$ *mm*
Tool step: A_1A_2 in tool path 1, and step length: 3.68		
Proposed approach	0.1	0 %
Circular arc approximation method	0.1	0 %
Chordal deviation method	0.0667	-33.3 %
Tool step: B_1B_2 in tool path 2, and step length: 3.81		
Proposed approach	0.1	0 %
Circular arc approximation method	0.0980	-2 %
Chordal deviation method	0.0670	-33 %
Tool step: C_1C_2 in tool path 3, and step length: 4.25		
Proposed approach	0.1	0 %
Circular arc approximation method	0.0926	-7.4 %
Chordal deviation method	0.0679	-32.1 %
Tool step: D_1D_2 in tool path 4, and step length: 5.19		
Proposed approach	0.1	0 %
Circular arc approximation method	0.0845	-15.5 %
Chordal deviation method	0.0692	-30.8 %
Tool step: E_1E_2 in tool path 5, and step length: 7.34		
Proposed approach	0.1	0 %
Circular arc approximation method	0.0757	-24.3 %
Chordal deviation method	0.0704	-29.6 %
Tool step: F_1F_2 in tool path 6, and step length: 10.72		
Proposed approach	0.1	0 %
Circular arc approximation method	0.0709	-29.1 %
Chordal deviation method	0.0713	-28.7 %

To understand the fidelity of the two established approximation methods, a NURBS surface is used and shown in Fig. 2.9. A ball end-mill with a diameter of 25.4 *mm* is used in machining, and the surface tolerance is 0.1 *mm*. Five tool steps are chosen and their corresponding pairs of CC points are labelled as A_1A_2, B_1B_2, C_1C_2, D_1D_2, and E_1E_2 shown in Fig. 2.9. The three methods of machining-error predictions are used to calculate the machining errors in each of the five tool steps, and the maximum machining error of each local surface area is recorded in Table 2.2.

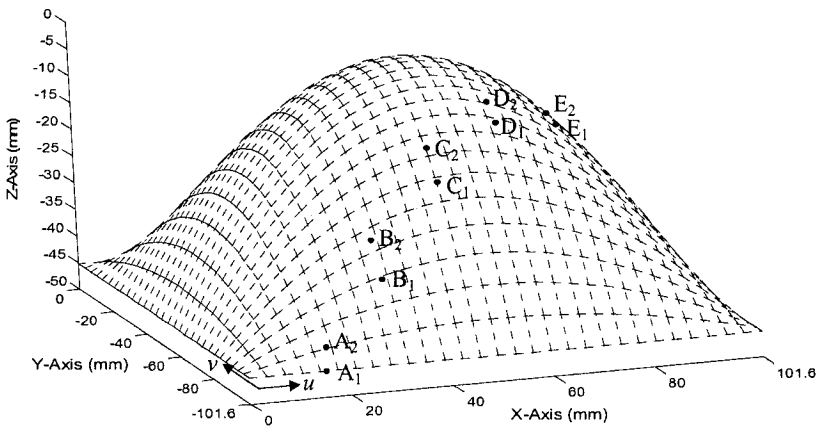

Figure 2.9 Selected CC points of five tool steps on the NURBS surface.

Table 2.2 Predicted maximum machining errors of the local surface areas using different methods

Unit: *mm*	Maximum machining error	Prediction deviation
Tool step 1: from $A_1(u = 0.15,\ v = 0)$ to A_2, and step length: 6.59		
Proposed approach	0.1	0 %
Circular arc approximation method	0.0472	-52.8 %
Chordal deviation method	0.0445	-55.5 %
Tool step 2: from $B_1(u = 0.3,\ v = 0.1)$ to B_2, and step length: 8.29		
Proposed approach	0.1	0 %
Circular arc approximation method	0.0783	-21.7 %
Chordal deviation method	0.0796	-20.4 %
Tool step 3: from $C_1(u = 0.45,\ v = 0.2)$ to C_2, and step length: 7.13		
Proposed approach	0.1	0 %
Circular arc approximation method	0.0859	-14.1 %
Chordal deviation method	0.0849	-15.1 %
Tool step 4: from $D_1(u = 0.6,\ v = 0.3)$ to D_2, and step length: 5.50		
Proposed approach	0.1	0 %
Circular arc approximation method	0.0900	-10 %
Chordal deviation method	0.0800	-20 %
Tool step 5: from $E_1(u = 0.75,\ v = 0.4)$ to E_2, and step length: 5.84		
Proposed approach	0.1	0 %
Circular arc approximation method	0.1285	28.5 %
Chordal deviation method	0.1036	3.6 %

In Table 2.2, the maximum machining errors in different tool steps predicted by using the chordal deviation method and the circular arc approximation method are different from those of this proposed approach. In the first tool step A_1A_2, the predicted

machining errors of the two established methods are 0.0472 and 0.0445 *mm*, respectively, which are far less than the accurate prediction of this proposed approach by 53% and 55%, respectively. The main reason for these low prediction accuracy is that the surface normals at the A_1 and A_2 are quite different and cannot meet the assumptions of these methods.

Through the comparison of predicted machining errors, it has demonstrated that using these established methods the machining errors cannot be accurately predicted at some locations for sculptured surface machining. This proposed approach can predict the machining errors more accurately and should be used for machining accurate sculptured surfaces.

Chapter 3 Application: CC Point Optimization System

In the previous chapter, it is proven that the newly proposed approach can predict machining errors more accurately than the established methods. In this chapter, a new system, based on the accurate predictions of machining errors, is proposed for the optimization of CC points on tool paths. First, two established CC point generation methods, the chordal deviation method and the circular arc approximation method, are introduced, and their limitations are addressed. Second, a sensitivity study of the machining errors with respect to cutting tools is conducted. Then a system implementing the generic, geometric approach to accurate machining-error predictions is proposed to optimize CC points on the tool paths. Finally, this CC point optimization system is applied to two practical parts to demonstrate its advantages over the two established methods.

3.1 Introduction to two established CC point generation methods

To optimize CC points in the step length determination, accurate prediction of machining errors is essential. If machining errors are not predicted accurately, the cutting tool may

gouge the surface when it moves through the CC points in a point-to-point way. At present, the CC points are determined using either the chordal deviation method [19, 27] or the circular arc approximation method [17, 18], which are widely used in industry. To understand their limitations, these established methods are examined in detail.

3.1.1 The chordal deviation method and circular arc approximation method

The chordal deviation method is simple but inaccurate. To illustrate this method, a diagram with a surface and four CC points on a tool path is illustrated in Fig.3 1. In this method, the shortest distance between a point on the tool path and the chord connecting the two CC points CC_2 and CC_3 is regarded as the machining error at that point; and the maximum machining error in the tool motion (also the chordal deviation) is regarded as the surface accuracy of the machined area. However, since the calculated distances are usually not in the direction perpendicular to the surface (the chordal deviation is not in line with the surface normal in Fig. 3.1), the actual maximum machining error is not accurately predicted. Besides, this method only takes the tool path geometry into consideration, not the type and size of the cutting tool, which causes additional machining errors.

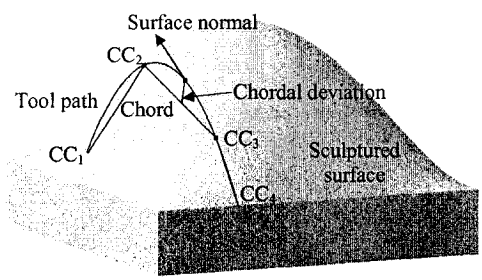

Figure 3.1 Illustration of the chordal deviation method.

An improved solution, the circular arc approximation method [21], takes both tool path and cutting tool geometries into consideration in predicting machining errors and calculates CC points with a simplified, estimate formula. This method builds a 2D model of machining errors (shown in Fig. 3.2) by approximating the tool path between two CC points (CC_1 and CC_2) with a planar circular arc and the surface normals with the normals of the circular arc at CC_1 and CC_2.

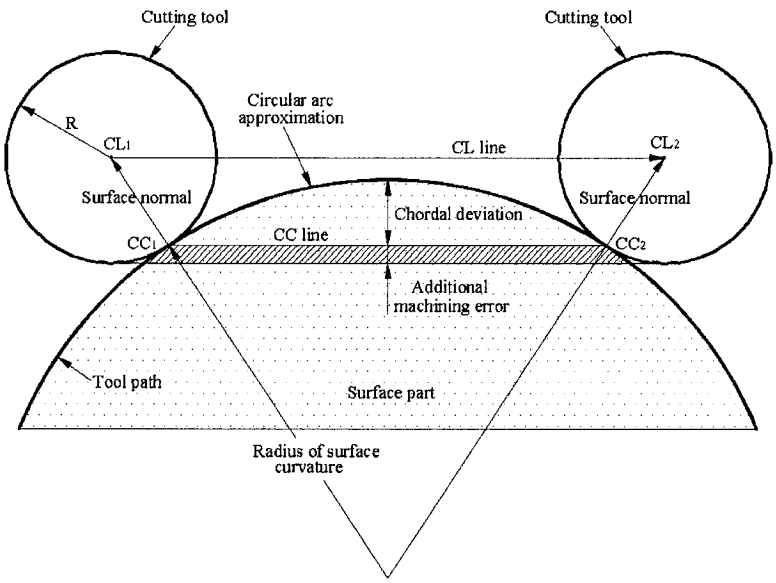

Figure 3.2 Model of machining errors in the circular arc approximation method.

This diagram shows when the tool moves from the cutter location (CL_1) of CC_1 to the cutter location (CL_2) of CC_2, the maximum machining error is the sum of the chordal deviation and the additional machining error. The CC point CC_2 can be adjusted so that the maximum machining error is equal to the tolerance. This method can calculate CC points accurately for conventional geometries, such as cylinders,

spheres, and 2D profiles. However, it cannot be used for sculptured surface machining.

3.1.2 Limitations of the established CC point generation methods

Sculptured surfaces are more complex in shape, compared to the conventional geometries. The main geometric feature of the sculptured surfaces is that their curvature at any surface point varies in all directions, so the orientation of the surface normal varies at different surface points. Figure 3.3 shows an iso-parametric tool path on a sculptured surface and a cutter located at two adjacent CC points, CC_1 and CC_2, on the tool path. As usual, the surface normals $\mathbf{n}_{CC_1}$ at CC_1 and $\mathbf{n}_{CC_2}$ at CC_2 are not on the same plane as CC_1 and CC_2, neither are the cutter locations CL_1 and CL_2. However, the circular arc approximation method assumes the surface normal as the circular arc normal and all surface normals are on the same plane. These assumptions are improper for sculptured surfaces. As a result, this method cannot predict machining errors accurately. Therefore, the chordal deviation and the circular arc approximation methods are not suitable to compute CC points of sculptured surfaces.

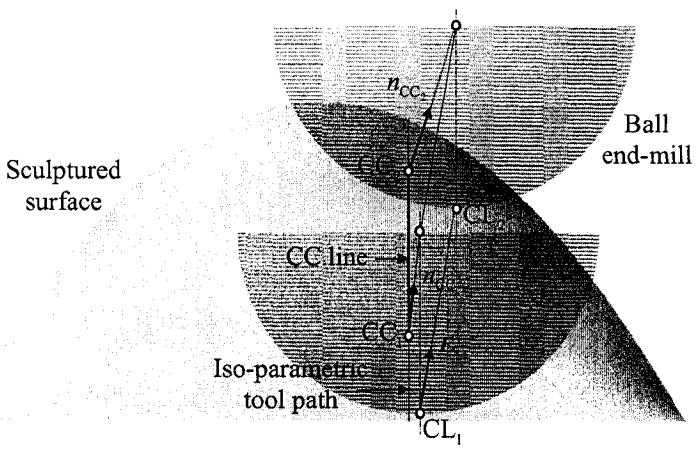

Figure 3.3 Geometric characteristics of sculptured surface milling.

The generic, geometric approach to accurate machining-error predictions (proposed in chapter 2 of this thesis) overcomes the limitations of the two established CC point generation methods and can predict machining errors accurately. To know the fidelity of the two established methods, these three are applied to the same sculptured surface; and the predictions of the machining errors at several locations are provided. It has been found that the predicted machining errors at point A using the chordal deviation method and the circular arc approximation method are less than the accurately-predicted machining errors by 53% and 55%, respectively (see Table 2.2 in the chapter 2 of this thesis). To optimize the CC points in sculptured surface machining, the approach to accurate prediction should be implemented. Using this approach, the relationship between machining error and end-mills can be found.

3.2 Sensitivity study of machining error with respect to tools

Since machining errors are related to the cutting tools, it is necessary to take the shape and size of the tools into account in the process of optimizing CC points. By applying this generic approach to accurate machining-error predictions, a sensitivity study can be conducted with respect to cutting tools.

3.2.1 Relationship between machining error and tool type

One application of this new approach is to verify that machining errors are related to the selected tool type. A semi-cylinder and a typical sculptured part are designed to show the relationship. To machine the two parts, three different types of end-mills such as flat, ball, and torus end-mills, are chosen (see Table 3.1 and 3.2). The diameters of all the tools are 25.4 *mm*, and the corner radius of the torus end-mill is 5.08 *mm*. For general purposes, pairs of cutter contact points are selected to represent different tool motions. In the machining of the semi-cylindrical surface, six pairs of CC points are designated with the same starting point A to represent five corresponding tool motions and labelled as AB, AC, AD, AE, AF, and AG in Fig. 3.4. Also in the machining of the sculptured surface, five pairs of CC points are selected and labelled as A_1A_2, B_1B_2, C_1C_2, D_1D_2, and E_1E_2 in Fig. 3.5. This new approach is applied to predict the machining errors at these CC points on the two surfaces. In each selected tool motion, the maximum machining errors between the two CC points are calculated for the three tools and are listed in Table 3.1 and Table 3.2. For example, in the machining of the semi-cylinder, the machining errors for the same cutting tool in the different tool motions are almost the same. However, in each

tool motion, the machining errors are different for three different cutting tools. The machining error of the flat end-mill and the ball end-mill are 0.0995 *mm* and 0.1493 *mm*, respectively. Therefore, the difference between the machining errors of the two end-mills is 50%. Also from table 3.2, the results of the three cutting tools are not the same in each tool step. The machining error of the flat end-mill is 0.0993 *mm*, and that of the ball end-mill is 0.1142 *mm* in C_1C_2, so the difference between the machining errors of the two end-mills reaches the maximum at 15%. It has been verified that flat, ball, and torus end-mills with the same size make different machining errors when they cut along the same CC points of a sculptured surface.

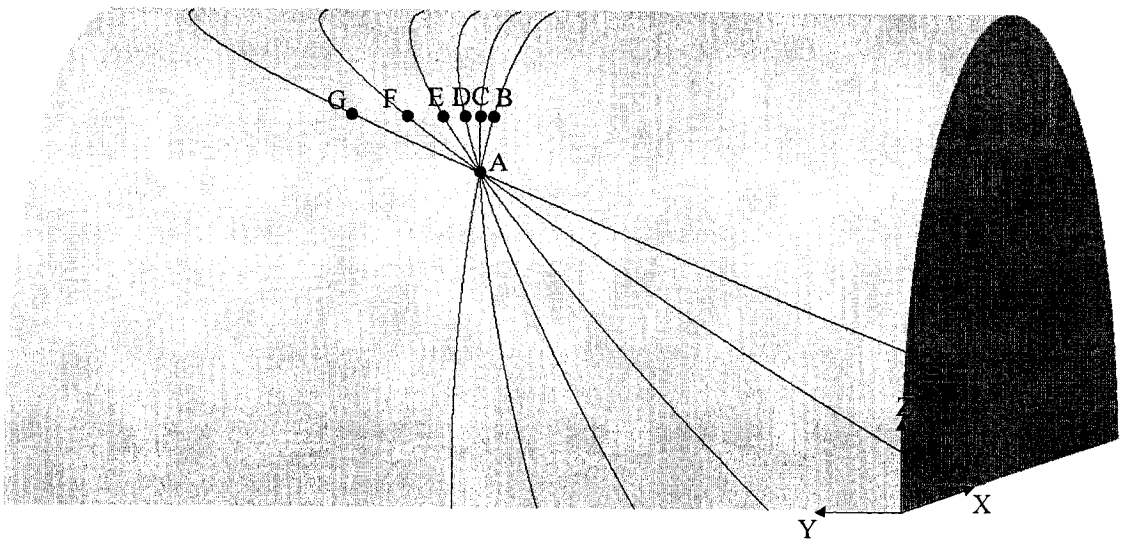

Figure 3.4 Six pairs of sample CC points on the semi-cylindrical surface in the sensitivity study.

Table 3.1 Maximum machining errors using the three tools in the selected tool steps for the semi-cylindrical surface machining

Unit: *mm*	Machining tolerance: 0.1	Tool diameter: $D = 25.4$		
Selected CC points in tool steps		Flat end-mill	Ball end-mill	Torus end-mill (corner radius: $r = 5.08$)
$A(7.44, 25.4, 17.96)$	$B(10.85, 25.4, 20.82)$	0.0995	0.1463	0.1170
	$C(10.88, 26.17, 20.84)$	0.0995	0.1492	0.1194
	$D(10.88, 27.06, 20.84)$	0.0995	0.1494	0.1194
	$E(10.88, 28.28, 20.84)$	0.0995	0.1493	0.1194
	$F(10.88, 30.39, 20.84)$	0.0995	0.1492	0.1194
	$G(10.88, 33.32, 20.84)$	0.0996	0.1492	0.1194

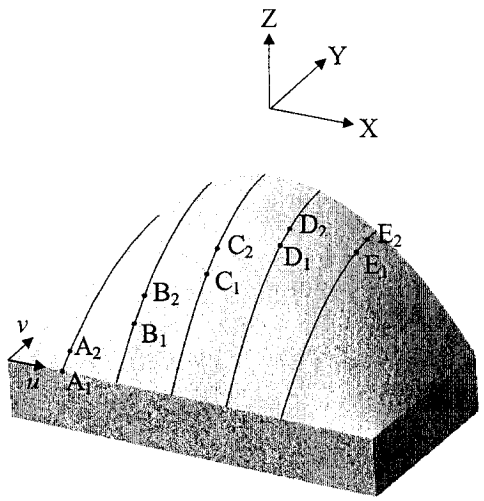

Figure 3.5 Five pairs of sample CC points on the sculptured surface in the sensitivity study.

Table 3.2 Maximum machining errors using the three tools in the selected tool steps for the sculptured surface machining

Unit: *mm*	Machining tolerance: 0.1		Tool diameter: $D = 25.4$	
Selected CC points in tool steps		Flat end-mill	Ball end-mill	Torus end-mill (corner radius: $r = 5.08$)
$A_1(u = 0.15,\ v = 0)$	$A_1(15.24,\ -101.6,\ -45.21)$ $A_2(15.24,\ -97.15,\ -41.28)$	0.0998	0.0807	0.0922
$B_1(u = 0.3,\ v = 0.1)$	$B_1(30.48,\ -91.44,\ -31.47)$ $B_2(30.48,\ -85.88,\ -25.32)$	0.0997	0.0996	0.0996
$C_1(u = 0.45,\ v = 0.2)$	$C_1(45.72,\ -81.28,\ -16.7)$ $C_2(45.72,\ -75.74,\ -11.49)$	0.0993	0.1142	0.1134
$D_1(u = 0.6,\ v = 0.3)$	$D_1(60.96,\ -71.12,\ -9.06)$ $D_2(60.96,\ -66.25,\ -6.22)$	0.0996	0.1049	0.1018
$E_1(u = 0.75,\ v = 0.4)$	$E_1(76.21,\ -60.96,\ -12.87)$ $E_2(76.20,\ -55.49,\ -11.83)$	0.0996	0.0904	0.0960

3.2.2 Relationship between machining error and tool size

With this proposed, accurate approach, a sensitivity study of machining errors in terms of the tool size is conducted to find the relationship between machining error and tool size. On the sculptured surface used in the previous section, five pairs of CC points are selected similarly (see Fig. 3.5). First, six ball end-mills with different sizes are chosen to machine the surface at the selected CC points. Using this approach, the machining errors are predicted in the tool motions, and the maximum machining error in each tool motion is listed in Table 3.3. It is easy to find that in each tool motion, the machining error using a bigger tool is greater than that of a smaller one. Moreover, if the surface normal changes dramatically at two CC points in a tool step, the difference between the maximum machining errors using the bigger and smaller tools is significantly larger for that step. For instance, the difference of the surface normal at A_1 and A_2 is larger than that at C_1 and C_2. In step A_1A_2, the maximum machining error of 0.2085 *mm* using the 76.2 *mm* tool is 3.174 times the error of 0.0657 *mm* generated by the 9.525 *mm* tool. This compares to the error variation in step C_1C_2, where the error (0.1298 *mm*) using the larger tool is 1.4 times the error (0.0920 *mm*) using the smaller tool.

Table 3.3 Maximum machining errors using ball end-mills of different sizes in the selected steps

Unit: *mm*	Diameters of ball end-mills					
Machining tolerance: 0.1	9.525 (3/8")	12.7 (0.5")	25.4 (1")	38.1 (1.5")	50.8 (2")	76.2 (3")
A_1(15.24, −101.6, −45.21) A_2(15.24, −96.65, −40.86)	0.0657	0.0725	0.0997	0.1269	0.1541	0.2085
B_1(30.48, −91.44, −31.47) B_2(30.48, −85.88, −25.32)	0.0860	0.0892	0.0996	0.1104	0.1215	0.1434
C_1(45.72, −81.28, −16.7) C_2(45.72, −76.10, −11.80)	0.0920	0.0921	0.0997	0.1072	0.1147	0.1298
D_1(60.96, −71.12, −9.06) D_2(60.96, −66.38, −6.28)	0.0856	0.0884	0.0995	0.1106	0.1216	0.1436
E_1(76.21, −60.96, −12.87) E_2(76.20, −55.22, −11.80)	0.0866	0.0893	0.0995	0.1096	0.1198	0.1400

Second, flat end-mills with different diameters are used to cut the same surface in the five selected tool motions. The maximum machining errors in the same tool steps are calculated using this proposed approach, and the results are recorded in Table 3.4. Similar to those of the ball end-mills, the maximum machining error of a bigger flat end-mill is always larger than that of a smaller one. This is also true for torus end-mills.

Table 3.4 Maximum machining errors using flat end-mills of different sizes in the selected steps

Unit: *mm*	Diameters of flat end-mills					
Machining tolerance: 0.1	9.525 (3/8")	12.7 (0.5")	25.4 (1")	38.1 (1.5")	50.8 (2")	76.2 (3")
A_1(15.24, −101.6, −45.21) A_2(15.24, −97.15, −41.28)	0.0603	0.0682	0.0998	0.1314	0.1629	0.2255
B_1(30.48, −91.44, −31.47) B_2(30.48, −85.88, −25.32)	0.0860	0.0887	0.0997	0.1106	0.1215	0.1433
C_1(45.72, −81.28, −16.7) C_2(45.72, −75.75, −11.5)	0.0977	0.0984	0.0993	0.1005	0.1017	0.1042
D_1(60.96, −71.12, −9.06) D_2(60.96, −66.25, −6.22)	0.0883	0.0906	0.0996	0.1087	0.1178	0.1359
E_1(76.21, −60.96, −12.87) E_2(76.20, −55.49, −11.84)	0.0795	0.0842	0.0996	0.1138	0.1278	0.1550

In industry, people often think that gouging only occurs on concave surfaces, not on convex surfaces and that it is always better to choose larger tools in convex surface machining for higher cutting efficiency. On the contrary, this study clearly shows that for a selected bigger tool, the tool will gouge the convex surfaces if the CC points are not determined properly. Therefore, this conventional thinking is not always true in sculptured surface machining.

3.3 CC point optimization system

An important application of this proposed approach is to optimize CC points on the tool paths for sculptured surface machining. Optimizing CC points is highly demanded in industry because the salient feature of using these points is that the cutting efficiency is high and the surface accuracy meets the tolerance. Since this approach is able to predict the machining errors accurately, a new software system for CC point optimization is made by implementing this approach. The objective of this optimization is to maximize the distance between two adjacent CC points (or the length of each tool step), but subject to a constraint that the machining errors cannot exceed the tolerance. Because the closed-form equation for accurate predictions of the machining errors cannot be found, the conventional optimization methods that require explicit, mathematic expressions of the objective function and the constraint cannot be used. In this work, the basic optimization technique is employed, and the optimization procedure is provided in the following.

3.3.1 Optimization procedure

In this new CC point optimization system, all steps, except the last one, along a tool path are optimized. To find a CC point based on its previous one, a line search technique is used to ensure the maximum machining error in this tool step is equal to the tolerance; and this line search always converges. For the last tool step, usually the machining error is less than the tolerance, so this step cannot be optimized. Specifically, the optimization procedure is listed as follows.

1) Starting from the first point of a tool path as the first CC point of a tool motion CC_1, assume a point on the tool path as the second CC point of the tool motion CC_2 and calculate the machining error.
2) If the machining error is greater than the tolerance, choose a point closer to CC_1 as CC_2. If the machining error is less than the tolerance, move the point farther to CC_1 as CC_2. If the machining error is equal to the tolerance, the point is the right CC point CC_2.
3) If the newly found CC point is not the ending point of the tool path, assign the newly found CC_2 as the first CC point of the next tool motion and go to step 1 for CC_2.
4) If the newly found CC point is the ending point of the tool path and the tool paths have not been finished, take the next tool path and go to step 1; otherwise, end the program.

3.3.2 Case study and analysis

To demonstrate this optimization system outperforms two established CC point determination methods, the chordal deviation and the circular arc approximation methods, two example parts are used, the first being a semi-cylinder and the second having a sculptured surface. This semi-cylinder is designed with a diameter of 25.4 *mm* and a length of 50.8 *mm* as shown in Fig. 3.6, and the tolerance is 0.01 *mm*. A ball end-mill of a diameter of 25.4 *mm* is used along with the planned, iso-parametric tool paths, and these three methods are applied to the tool paths for CC points (see Fig. 3.6). Since the circular arc approximation method can accurately predict the

machining errors for this simple part, it determines the same CC points as those of the optimization system. Both of these methods are applied to the right-hand region of the cylindrical surface, and thirty-six CC points on each tool path are obtained (see Fig. 3.7(a)). The chordal deviation method is applied to the tool paths on the left-hand region, and twenty-nine CC points are calculated on each tool path as shown in Fig. 3.7(b).

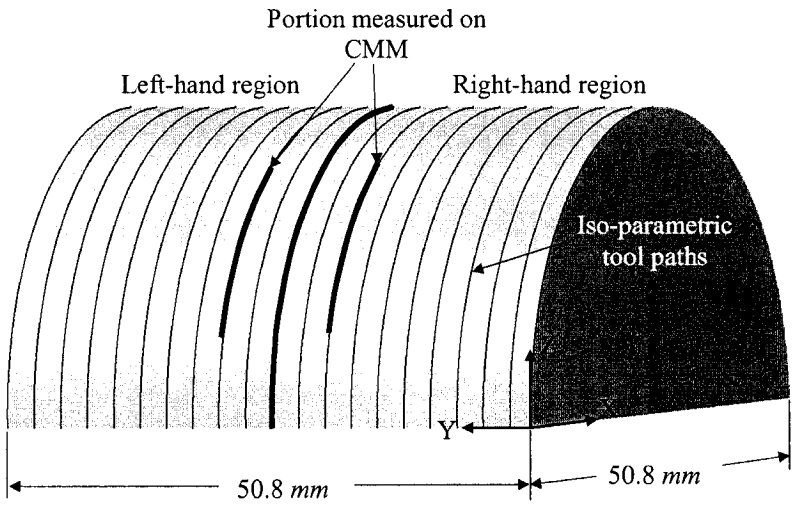

Figure 3.6 Semi-cylindrical surface part with iso-parametric tool paths.

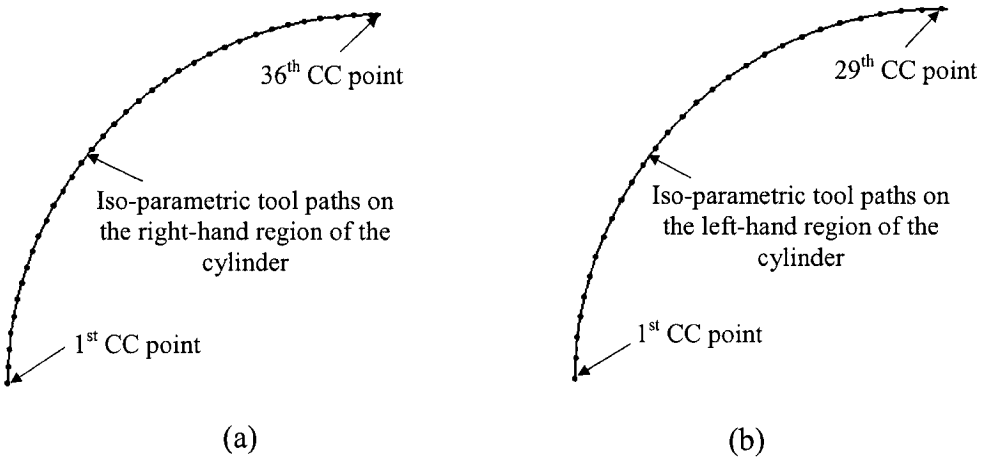

Figure 3.7 CC points on a tool path determined by (a) the circular arc approximation method or the optimization system; (b) the chordal deviation method.

For comparison, the right- and left-hand regions of the surface are machined with their CC points calculated with these respective methods. The machining is simulated with the CATIA software, and the simulation results are shown in Fig. 3.8. In this diagram, area A is enlarged to show that the surface accuracy is different in these two regions. To find the surface accuracy, the approach proposed in chapter 2 of this thesis is then used to accurately predict the machining errors at 3535 sample points along one tool path from the two regions; and the results are shown in Fig. 3.9. In this diagram, the black solid and blue dotted lines represent the machining errors of the right- and left-hand regions, respectively. The maximum machining error of the right-hand region is at the tolerance of 0.01 *mm*; however, gouging occurs on the left-hand region, where the error reaches 0.015 *mm*.

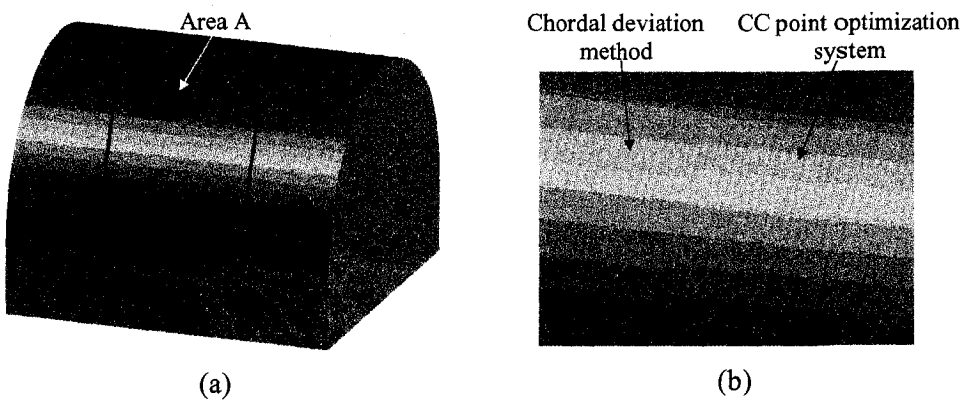

Figure 3.8 Machined surface of the semi-cylinder in simulation.

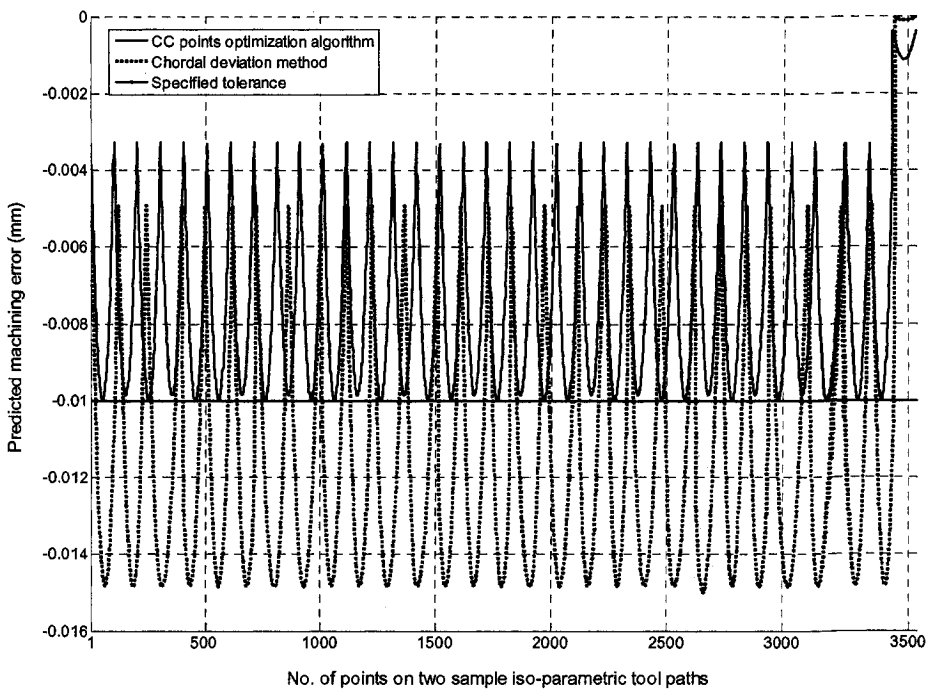

Figure 3.9 Predicted machining errors at the sample points along one tool path from the two regions.

This part is then machined on a Deckel Maho 60T CNC milling machine. The part material is 6061T aluminium, and the cutting tool is a high speed steel ball end-mill with a diameter of 25.4 *mm*. The spindle speed and feed rate are 1,500 *rpm* and 250 *mm/min* respectively, values which are conservative in order to reduce cutting tool deflection and vibration. Based on the calculated CC points, the part is machined and shown in Fig. 3.10(a). Specifically, the right-hand region is machined with the CC points optimized by the new system, and the left-hand region with the ones determined by the chordal deviation method. To verify this optimization system is more accurate than the chordal deviation method, the machined part is inspected on a Mitutoyo LEGEX 9106 coordinate measurement machine (CMM) with an accuracy of 0.1 micro (see Fig. 3.10(b)) to confirm the predicted machining errors.

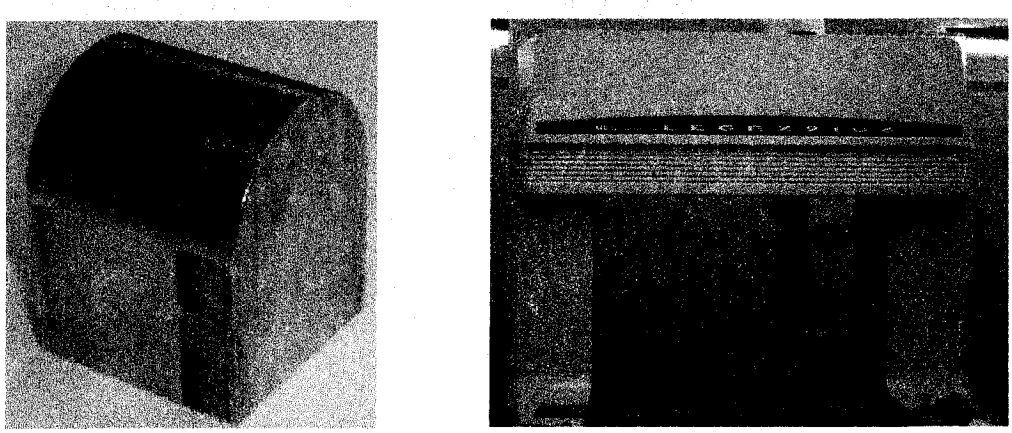

(a) (b)

Figure 3.10 (a) Machined semi-cylindrical surface part; (b) the semi-cylindrical surface part measured on a CMM.

The portions of the right- and left-hand regions are measured (see Fig. 3.6) for actual machining errors that are plotted in Fig. 3.11 and 3.12, respectively. In these graphs, the measurements of the machining errors vary along a tool path in a general wave form, complying with the pattern of their predictions in Fig. 3.9. Because of the noise from other sources in machining, the error deviates in a small range along the wave pattern. In details, the measured value of the maximum machining error in the left-hand region is equal to the predicted result at 0.015 *mm*. Actually, this region is gouged at the locations, where the machining errors are larger than the tolerance (0.01 *mm*). In contrast, all of the measurement data for the right-hand region are less than the tolerance, except those at some locations between points 1090 and 1200. The reason for this has not been identified yet. Meanwhile, the maximum machining error of this region is close to the tolerance in general. This inspection verifies that the CC-point-optimization system and the accurate machining-error-prediction approach proposed in this paper are reliable.

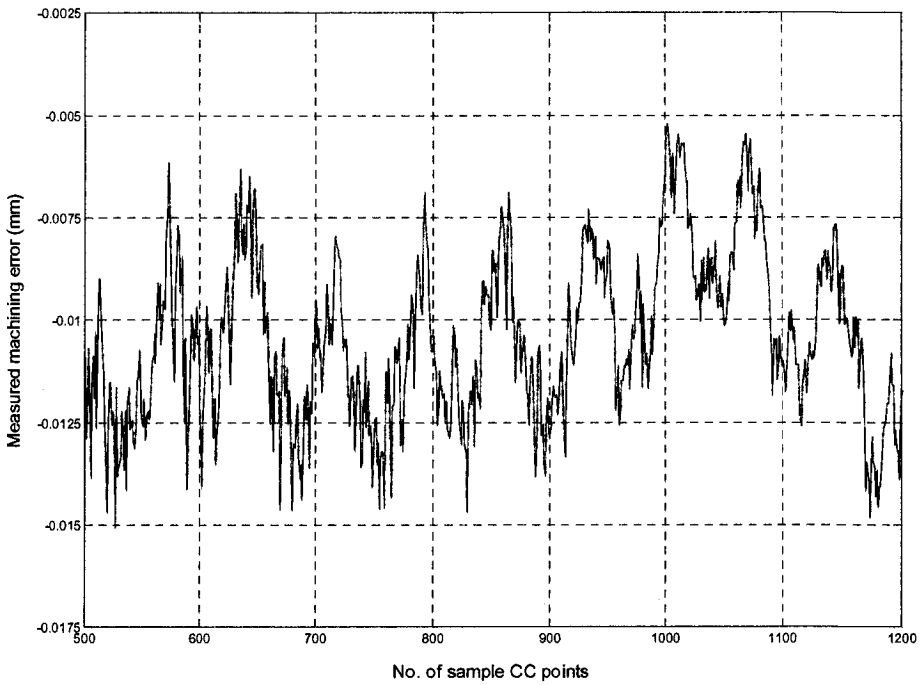

Figure 3.11 Measured machining errors of the left-hand region

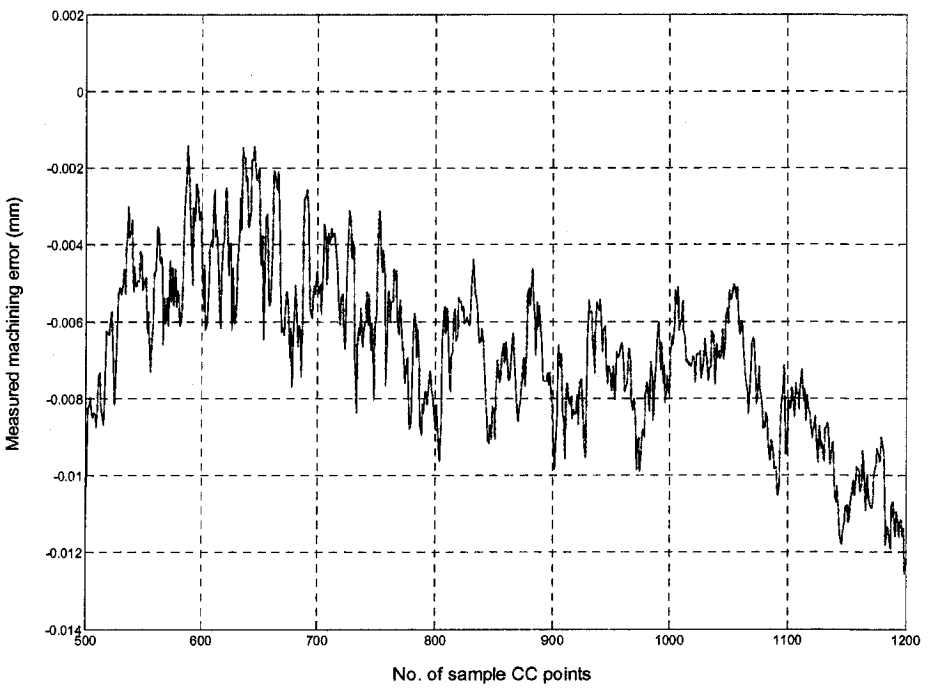

Figure 3.12 Measured machining errors of the right-hand region.

In the second example, the sculptured surface used in the section 2 of this chapter is adopted with a tolerance specified as 0.2 *mm* for demonstration purposes (see Fig. 3.13). To machine this surface, an iso-parametric tool-path pattern is first selected, and an appropriate number of tool paths are then chosen as shown in Fig. 3.13. Similar to the example of semi-cylinder, the three methods of CC point determination are applied to each of the planned tool paths. Because of the close results of using the chordal deviation and the circular arc approximation methods in this case, only those CC points calculated by the later are displayed in Fig. 3.13(a). The CC points determined by the optimization system are shown in Fig. 3.13(b). In particular, five CC points are determined on the outermost tool paths by the chordal deviation and the circular arc approximation methods, whereas six points by the optimization system. However, the numbers of CC points on any inner tool path are the same using these different methods despite of the different locations of the points.

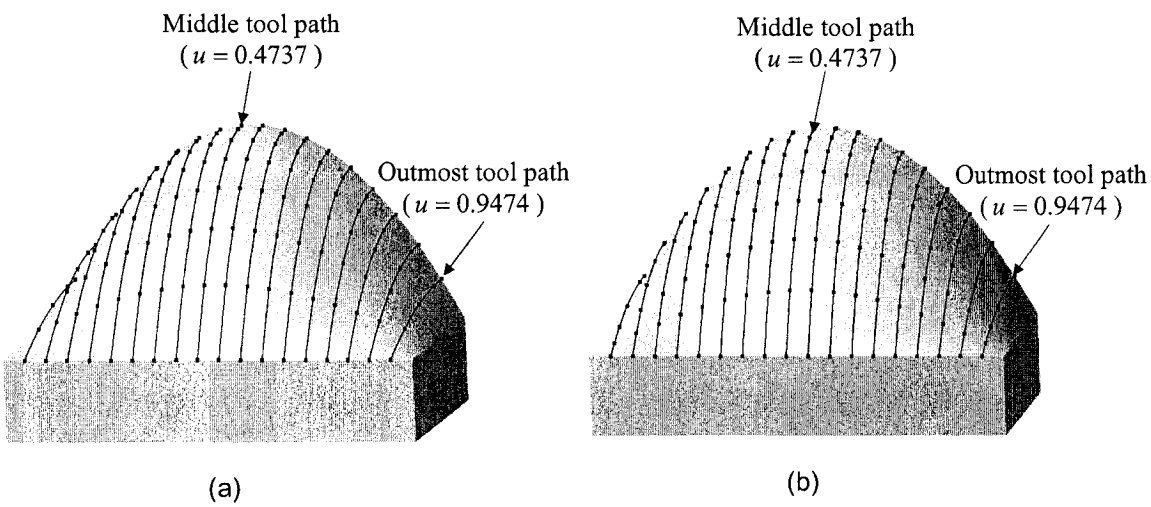

Figure 3.13 CC points on iso-parametric tool paths of the sculptured surface determined by (a) the circular arc approximation method; (b) the CC point optimization system.

The CC points computed by the three methods are used in machining simulations on CATIA software, and the resulting parts are shown in Fig. 3.14, 3.15, and 3.16, respectively. Region A in each of these figures is enlarged to show the machined surface in detail. It is easy to observe that the surface accuracy along the outmost tool path (shown in region B) in Figs. 3.14 and 3.15 is worse than that (in region B) of Fig. 3.16. To find accurate machining-error predictions along the middle and outmost tool paths ($u = 0.4737$ and $u = 0.9474$; $v \in [0, 0.5]$), 820 and 505 sample points are selected on the two paths respectively by changing the value of v; the new approach to machining-error predictions is used, and the results are shown in Fig. 3.17 and Fig. 3.18. In these two figures, the black solid line represents the machining errors of the part machined with the CC points optimized using this new system, and the maximum machining errors are close to the tolerance. The red solid line denotes the specified machining tolerance. The green dash line is for the chordal deviation method, and the blue dotted line is for the circular arc approximation method. In Fig. 3.17, the maximum machining errors of the chordal deviation and circular arc approximation methods are 0.255 *mm* and 0.25 *mm*, respectively, which are close to the specified tolerance of 0.2 *mm*; however, as can readily be seen in Fig. 3.18, the errors of the part machined with the CC points optimized by the optimization system are within the tolerance; whereas, the maximum machining error of the chordal deviation method is 0.88 *mm* and that of the circular arc approximation method is 0.84 *mm*. Both of these values exceed the tolerance by more than 300%, thus gouging occurs on these two parts.

This example shows how CC points can be optimized by using the newly proposed optimization system, and that the chordal deviation and the circular arc approximation methods can cause gouging in sculptured surface machining.

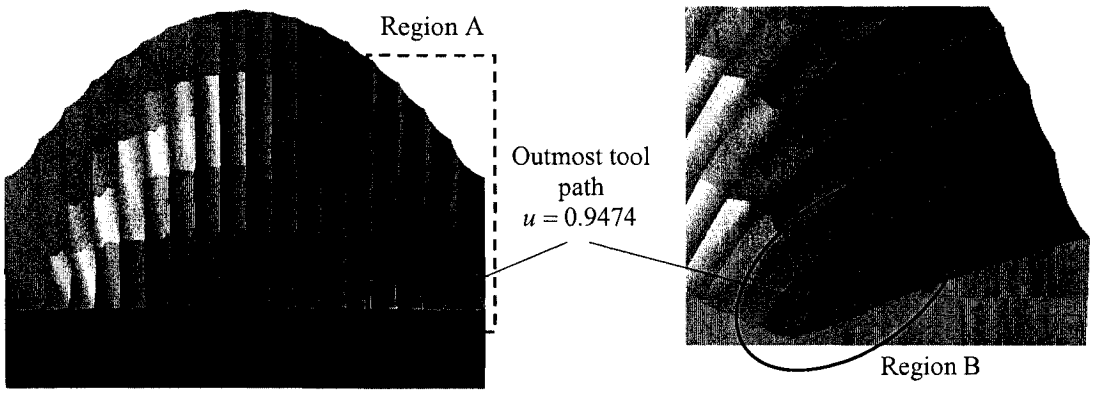

Figure 3.14 Sculptured surface machined with the CC points determined with the chordal deviation method.

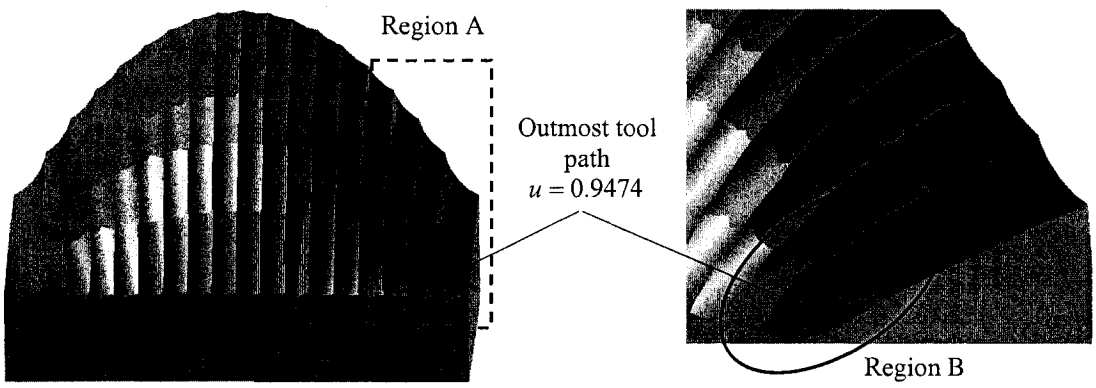

Figure 3.15 Sculptured surface machined with the CC points determined with the circular arc approximation method.

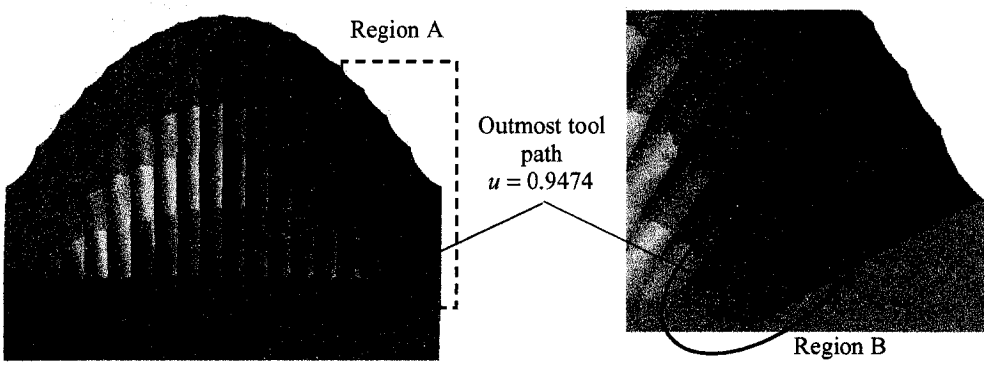

Figure 3.16 Sculptured surface machined with the CC points optimized with the CC point optimization system.

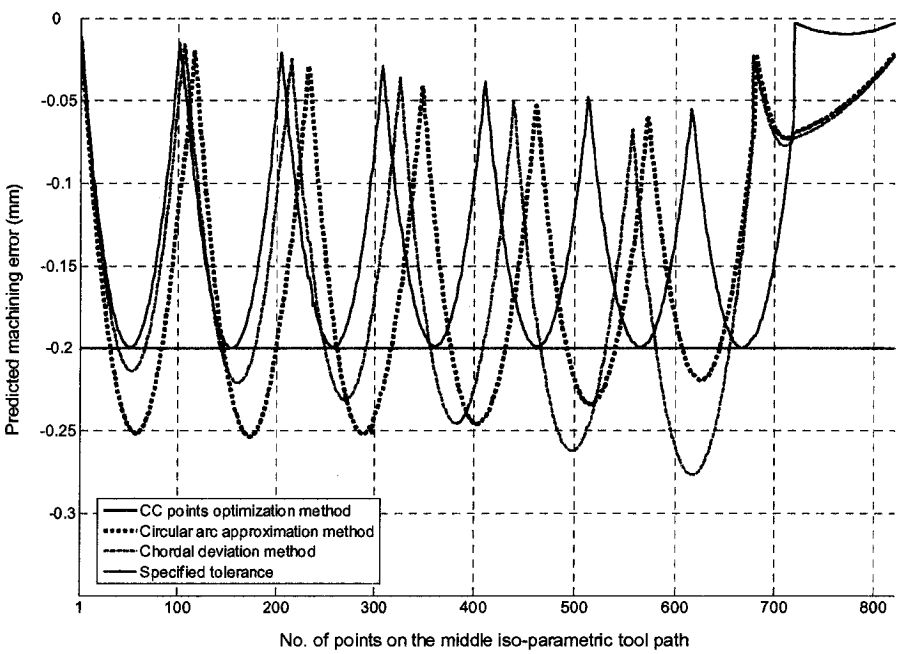

Figure 3.17 Predicted machining errors along the middle tool path using the three methods.

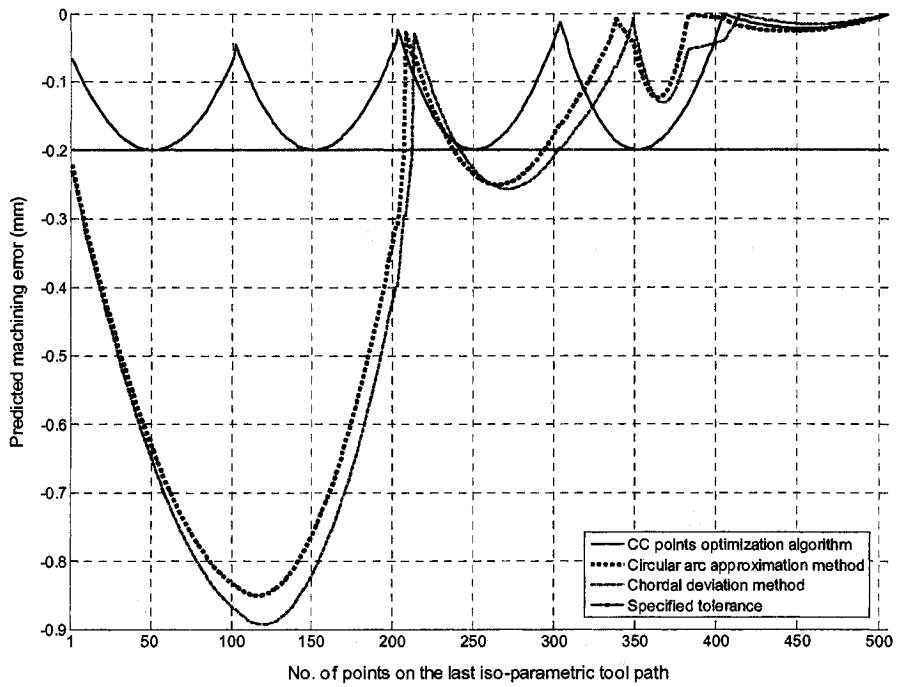

Figure 3.18 Predicted machining errors along the outmost tool path using the three methods.

In the CNC machining of the sculptured surface part, the material of this sculptured part is 6061 aluminium, and it is machined on DECKEL MAHO 60T CNC milling center. The specified surface tolerance is set as 0.06 *mm*. The path interval is defined as 0.5676 *mm* (around 180 tool paths over the whole surface). A high-speed-steel flat end-mill with diameter of 25.4 *mm* is used both in rough machining and in finish machining. The cutting feed rate is 500 *mm/min*, and the spindle speed is 1000 rpm. The machined part is shown in Figure 3.19.

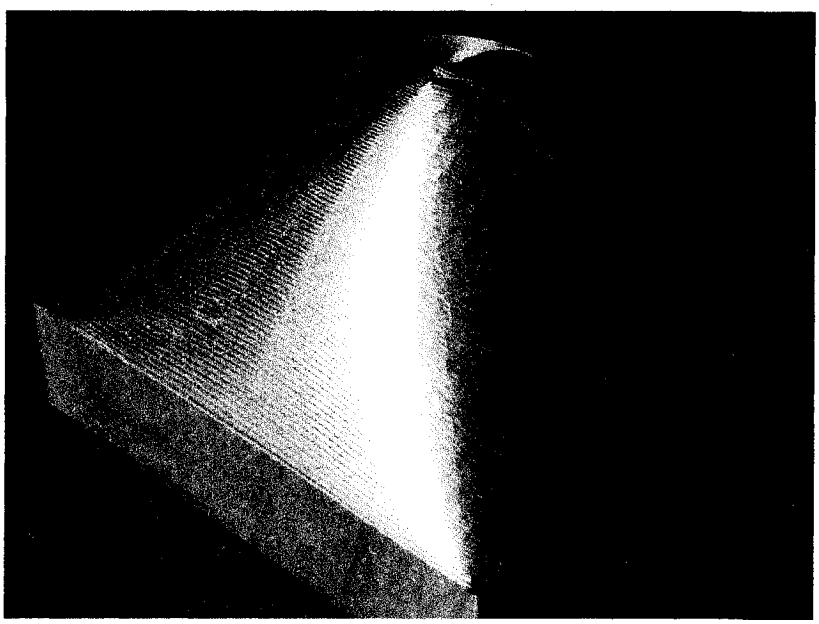

Figure 3.19 Machined part.

Chapter 4 Summary and Contributions

In the first part of this work, a new approach has been proposed to predict machining errors accurately in sculptured surface machining due to the tool-surface mismatch. By using the closed form equation of cutting circle envelop, the furrow patches can be found quickly and precisely. The accuracy of machining-error predictions is much higher than the prediction by the established approximation methods. This proposed approach can be used to determine gouging free cutter contact points on sculptured surfaces. It can also be used in machining simulation to facilitate representing the machining surface geometry.

Also, this thesis work has disclosed two relationships between machining error and cutting tool, including (a) that the machining error is different if different types of cutting tools with the same size are used, and (b) that the machining error is larger for the same CC points when bigger cutting tools are employed. This work has proposed a new system to optimize cutter contact points for sculptured surface machining based on the generic, geometric approach to accurate machining-error predictions. Two practical examples have demonstrated that this CC point optimization system can optimize cutting for sculptured surfaces, while the chordal deviation and the circular arc approximation

methods can gouge them. Thus this system can improve the accuracy of sculptured surface parts and can be directly implemented in the manufacturing industry.

The study results show that using this new proposed approach has increased the machining accuracy of the semi-cylinder (see Table 2.1) and the sculptured part (see Table 2.2) up to 30% and 55%, respectively. Significantly, based on the predicted machining errors by using this approach, the CC point optimization system determine the optimized CC points along tool paths by which the machined surface quality can be improved by more than 300%, compared to the chordal deviation and the circular arc approximation methods (see Fig.3.18).

In brief, this thesis research work provides a correct understanding of 3-axis CNC milling of sculptured surfaces, and lays a foundation for the research of machining sculptured surfaces with high quality.

Bibliography

1. Kunwoo, L., *Principles of CAD/CAM/CAE Systems*, Addison-Wesley, 1999.

2. Piegl, L., and Tiller, W., *The NURBS Book*, Springer, 1997.

3. Choi, B. K., and Jerard, R. B., *Sculptured surface machining: theory and applications*, Kluwer Academic Publishers, 1998.

4. Lim, E. M., Feng, H. Y., Menq, C. H., and Lin, Z. H., 1995, "The prediction of dimensional error for sculptured surface productions using the ball-end milling process. Part 1: Chip geometry analysis and cutting force prediction," *International Journal of Machine Tools and Manufacture*, Vol. 35, No. 8, pp. 1149 – 1169.

5. Lim, E. M., and Menq, C. H., 1995, "The prediction of dimensional error for sculptured surface productions using the ball-end milling process. Part 2: Surface generation model and experimental verification," *International Journal of Machine Tools and Manufacture*, Vol. 35, No. 8, pp. 1171 – 1185.

6. Feng, H. Y., and Menq, C. H., 1996, "A flexible ball-end milling system model for cutting force and machining error prediction," *Journal of Manufacturing Science and Engineering*, Vol. 118, pp. 461 – 469.

7. Yun, W. S., Ko, J. H., Cho, D. W., and Ehmann, K. F., 2002, "Development of a virtual machining system, part 2: prediction and analysis of a machined surface error," *International Journal of Machine Tools & Manufacture*, Vol. 42, pp. 1607 – 1613.

8. Ikua, B. W., Tanaka, H., Obata, F., and Sakamoto, S., 2001, "Prediction of cutting forces and machining error in ball end milling of curved surfaces – I theoretical analysis," *Precision Engineering, Journal of the International Societies for Precision Engineering and Nanotechnology*, Vol. 25, pp. 266 – 273.

9. Loney, G. C., and Ozsoy, T. M., 1987, "NC machining of free form surfaces," *Computer–Aided Design*, Vol. 19, No. 2, pp. 85 – 90.

10. Faux, I. D., and Pratt, M. J., *Computational geometry for design and manufacture*, Ellis Harwood Limited, 1979.

11. Wang, W. P., and Wang, K. K., 1986, "Geometric Modeling for Swept Volume of Moving Solids," *IEEE Computer Graphics and Applications*, Vol. 6, No. 12, pp. 8 – 17.

12. Altintas, Y., and Spence, A., 1991, "End milling force algorithm for CAD systems," *Annual CIRP*, Vol. 40, pp. 31 – 34.

13. Blackmore, D., Leu, M. C., and Wang, L. P., 1997, "The sweep-envelope differential equation algorithm and its application to NC machining verification," *Computer-Aided Design*, Vol. 29, No. 9, pp. 629 – 637.

14. Chung, Y. C., Park, J. W., Shin, H., and Choi, B. K., 1998, "Modeling the surface swept by a generalized cutter for NC verification," *Computer-Aided Design*, Vol. 30, No. 8, pp. 587 – 594.

15. Roth, D., Bedi, S., Ismail, F., and Mann, S., 2001, "Surface swept by a toroidal cutter during 5-axis machining," *Computer-Aided Design*, Vol. 33, No. 1, pp. 57 – 63.

16. Chiou, C. J., and Lee, Y. S., 2002, "Swept surface determination for five-axis numerical control machining," *International Journal of Machine Tools and Manufacture*, Vol. 42, pp. 1497 – 1507.

17. Choi, B. K., and Jerard, R. B., *Sculptured surface machining: theory and applications*, Kluwer Academic Publishers, 1998.

18. George, K. K., Ramesh B. N., 1995, "On the effective tool path planning algorithms for sculptured surface manufacture," *Computers & Industrial Engineering*, Vol. 28, No. 4, pp. 823 – 838.

19. Loney, G. C., and Ozsoy, T. M., 1987, "NC machining of free form surfaces," *Computer–Aided Design*, Vol. 19, No. 2, pp. 85 – 90.

20. Ding, S., Mannan, M. A., Poo, A. N., Yang, D. C. H., and Han, Z., 2003, "Adaptive iso-planar tool path generation for machining of free-form surfaces," *Computer-Aided Design*, Vol. 35, pp. 141 – 153.

21. Huang, Y., and Oliver, J. H., 1994, "Non-constant parameter NC tool path generation of sculptured surfaces," *International Journal of Advanced Manufacturing Technology*, Vol. 9, pp. 281 – 290.

22. Suresh, K., and Yang, D. C. H., 1994, "Constant scallop-height machining of free-form surfaces," *Journal of Engineering for Industry*, Vol. 116, No. 2, pp. 253 – 259.

23. Chen, Z. C., and Song, D., 2004, "A generic and practical algorithm of iso-cusped tool path planning for three-axis sculptured part CNC machining," *Transactions of the North American Manufacturing Research Institution/Society of Manufacturing Engineers*, Vol. 22, pp. 190 – 201.

24. Chen, Z. C., Vickers, G. W., and Dong, Z., 2004, "A new principle of tool path planning for sculptured surfaces – steepest-ascending tool paths in 3-axis CNC machining," *Journal of Manufacturing Science and Engineering, ASME Transactions*, Vol. 126, pp. 515 – 523.

25. Chen, Z. C., Vickers, G. W., and Dong, Z., 2003, "Integrated steepest-directed and iso-cusped tool path generation for three-axis CNC machining of sculptured parts," *Journal of Manufacturing Systems*, Vol. 22, No. 3, pp. 190 – 202.

26. Chung, Y. C., Park, J. W., Shin, H., and Choi, B. K., 1998, "Modeling the surface swept by a generalized cutter for NC verification," *Computer-Aided Design*, Vol. 30, No. 8, pp. 587 – 594.

27. Faux, I. D., and Pratt, M. J., *Computational geometry for design and manufacture*, Ellis Harwood Limited, 1979.

Publications

- Cai, W., and Chen, Z.C., "Cutter contact points determination in 3-axis CNC milling of sculptured surfaces," *Proceedings of the Fifth International Workshop on Advanced Manufacturing Technologies*, 2005.
- Chen, Z.C., and Cai, W., "A generic, geometric approach to accurate machining-error predictions for 3-axis CNC milling of sculptured surface parts part I modeling and formulation," submitted to the *ASME Transactions of Journal of Manufacturing Science and Engineering*, 2005.
- Chen, Z.C., and Cai, W., "A generic, geometric approach to accurate machining-error predictions for 3-axis CNC milling of sculptured surface parts part II applications and analysis," submitted to the *ASME Transactions of Journal of Manufacturing Science and Engineering*, 2005.